CORROSION BEHAVIOR OF Zn-Ni COATINGS DEPOSITED BY ELECTROLYTIC PLASMA PROCESSING

by

GIANCARLO RIOS LOMBARDI

Presented to the Faculty of the Graduate School of

The University of Texas at Arlington in Partial Fulfillment

of the Requirements

for the Degree of

MASTER OF SCIENCE IN MATERIALS SCIENCE AND ENGINEERING

THE UNIVERSITY OF TEXAS AT ARLINGTON

December 2008

ACKNOWLEDGMENTS

I would like to express my sincere gratitude to Dr. E.I. Meletis, my thesis advisor for his advice, tenacious drive, help and valuable guidance throughout the whole research work. I would also wish to extend my most sincere appreciation to Dr. Shaoxin You for conducting the SEM/EDS analysis and x-ray diffraction experiments and analysis.

In addition, I wish to thank the personnel in the machine shop of the Mechanical Engineering Department at the University of Texas at Arlington for their help in the preparation of specimens and several other components needed during the experimental work.

Finally, I want to show appreciation to my parents and to other family members and friends for their friendship and support.

September 19, 2008

ABSTRACT

CORROSION BEHAVIOR OF Zn-Ni
COATINGS DEPOSITED BY
ELECTROLYTIC PLASMA
PROCESSING

Giancarlo Rios Lombardi, M.S.

The University of Texas at Arlington, 2008

Supervising Professor: Esthathios Meletis

In the current research project, three groups of Zn-Ni coatings of various Ni contents were deposited on comercial carbon steel by electrolytic plasma processing (EPP), a novel surface modification technique. The coating characteristics were studied along with their corrosion behavior in order to determine their potential as electroplated Cd coating replacements. The latter electroplated coatings are currently used in aerospace applications but are toxic and hazardous to humans and the environment.

Coating surfaces and cross sections were analyzed by scanning electron microscopy (SEM) while compositional analysis was conducted by energy-dispersive spectroscopy (EDS). Phase structure analysis was carried out by x-ray diffraction analysis. Corrosion behavior in tap water and 3.5% NaCl solution was studied by corrosion potential measurements and anodic polarization testing. The results showed that EPP can deposit conformal Zn-Ni coatings with various Ni contents by varying the zinc and nickel salt ratio in the electrolyte *via* an up normal co-deposition process (i.e., a 50 wt% Ni salt in the electrolyte results in 30 wt% Ni in the coating). The SEM observations showed that the coatings were composed of two phases with different morphologies; a nodular type and a flake type. The XRD analysis showed that the

nodular Zn-Ni phase was a γ_1 Zn-rich phase and the flake type phase a γ_2 Ni-rich phase. The γ_2 phase was present only in coatings with more than18 wt% Ni and its presence increased with increasing Ni content.

Analysis of the electrochemical tests showed an increase in the corrosion potential and a decrease in the corrosion current density with increasing Ni content in the coatings. As one might surmise, corrosion potential was found to be lower and corrosion rate higher in tests conducted in NaCl solution compared to tap water. Post electrochemical testing SEM observations showed that the γ_1, Zn-rich phase was most affected by corrosion compared to Ni-rich, γ_2 phase. These findings are in agreement with the XRD and EDS results since the higher Ni content phase is expected to be more noble than the active Zn-rich phase.

Comparisons with the electrochemical behavior of 4340 steel showed that only coatings with less than 18 wt% Ni (only γ_1 phase present) have a more active potential than that of steels in both tap water and NaCl solution, thus can serve as sacrificial anodes providing protection. Coatings with a higher Ni content (<18 wt% Ni) were found in general to be noble compared to steel (presence of the γ_2 phase), thus may accelerate corrosion of the underlying steel if the coating is damaged or cracked. The role of conversion coatings was found to be positive in improving the sacrificial behavior of the low Ni content coatings.

Thus, the present study clearly shows that Zn-Ni coatings with <18 wt% Ni deposited by EPP are anodic to steel providing corrosion protection by acting as sacrificial anodes. These coatings possess the potential to replace current electroplated Cd coatings. Finally, application of conversion coatings can provide additional benefits to the Zn-Ni coatings in their corrosion protection role.

TABLE OF CONTENTS

LIST OF ILLUSTRATIONS

LIST OF TABLES

CHAPTER 1

INTRODUCTION

Corrosion is an electrochemical degradation of materials that has tremendous effects on all segments of our economy ranging from the electronic industry to transportation and from energy to biomaterials applications. It is estimated that corrosion destroys one quarter of the world's annual steel production, which corresponds to about 150 million tons per year [1].

Metallic coatings can offer corrosion protection to the underlying metal from a corrosive environment by acting as sacrificial anodes (cathodic protection). Such protection requires a more active corrosion potential for the coating compared to the substrate material. Under these conditions, the coating corrodes preferentially and provides protection to the substrate even when exposed due to coating discontinuities or mechanical damage [2].

Cadmium has been used for years as a sacrificial coating in high-strength steels especially in aerospace industry. Currently, efforts are being made to find a suitable alternative to Cd coatings because of its toxicity and environmental hazard. Zinc-nickel alloy coatings are being extensively studied as a replacement for cadmium coatings since they are environmentally friendly with good corrosion resistance, superior formability and improved welding characteristics [3]. However, Zn-Ni alloys in general, have a more negative potential than Cd due to the high content of Zn in the alloy which dissolves rapidly in corrosive environments. Although Ni is more noble than Zn, for many traditional coating methods the co-deposition of Zn-Ni is anomalous and a higher percent of Zn is present in the final deposit. On the other hand, Ni is more noble than Fe and coating with a high Ni content may posses a higher potential and thus, accelerate corrosion. Thus there is a need for new deposition methods where the Ni content can be controlled [3].

Another challenge to overcome is that in the majority of applications for structural steel (aerospace, ships, marine structures, pipelines, bridge supports and industrial structures, etc.), cleaning is required prior to coating of the surface. Cleaning is needed firstly because steel is

covered by a layer of mill-scale (produced by the hot-rolling mill), other 'soil' and oil and grease contamination. Secondly, adhesion to base metal is of utmost importance to coating performance and is directly related to the cleanliness of the surface and the ability to develop an 'anchor' surface profile (surface with micro scale roughness) providing a key or mechanical interlocking for the coating.

Traditional methods of cleaning steel include: acid pickling and sand shot grit blasting. These conventional methods have major disadvantages (high energy cost, environmentally-unfriendly, disposal problems, unfavorable surface profile, etc). Electrolytic cleaning methods are known, but they have not been successfully commercialized since in their present state they are unable to remove mill-scale and other heavy contaminants. Likewise, current metal coating methods have several limitations. For example, electro- and electroless plating are relatively slow and typically use environmentally hazardous chemicals. Dipping and metal spraying methods are faster but the resulting coatings may have adhesion problems during bending and formation. Thus, there is a need at present for new, cost-effective cleaning and coating methods that can produce quality, long-lasting surfaces.

Electrolytic plasma processing (EPP) is a newly developed surface modification (cleaning and coating) method, develop by CAP Technologies (Baton Rougue, LA) that has the potential to overcome the above limitations of conventional methods, both for the cleaning and coating. In the present work, EPP was studied in relation to cleaning steel surfaces and depositing zinc-nickel (Zn–Ni) coatings as a potential alternative to Cd replacement [4,5].

CHAPTER 2

OBJECTIVES

Electrolytic plasma processing is a novel and environmentally friendly surface cleaning and coating method that has the potential to overcome limitations of present techniques. The main objective of the present work was to study the characteristics of various Zn-Ni coatings produced by electrolytic plasma processing and assess their potential as sacrificial anodes for steel and potential alternatives to electroplated Cd replacement.

CHAPTER 3

BACKGROUND

3.1 Electrochemical considerations

Corrosion can be defined as the degradation of a material due to a reaction with its environment. It is an electrochemical phenomenon involving the balance of two reactions, an anodic (site of oxidation) that releases electrons and a cathodic that consumes electrons (site of reduction) [6,7]. The anodic reaction is:

$$M \rightarrow M^{x+} + xe^{-} \quad \text{Reaction 1}$$

where M stands for a metal and x stands for the number of electrons that an atom of the metal will easily release. According to the environment where corrosion is taking place, the possible cathodic reactions can be:

$O_2 + 4H^+ + 4e^- \rightarrow 2H_2O$ (oxygen reduction in acidic solution) Reaction 2

$1/2O_2 + H_2O + 2e^- \rightarrow 2OH^-$ (oxygen reduction in neutral or basic solution) Reaction 3

$2H^+ + 2e^- \rightarrow H_2$ (hydrogen evolution from acidic solution) Reaction 4

$2H_2O + 2e^- \rightarrow H_2 + 2OH^-$ (hydrogen evolution from neutral water) Reaction 5

$M^{x+} + Ye^- \rightarrow M^{(x-Y)+}$ (Metal reduction) Reaction 6

The corrosion process is a result of thermodynamic instability. The first law of thermodynamics relates energy, work and heat. Assuming reversibility and constant temperature, pressure and volume, the system can be represented by $\Delta U = T\Delta S - nFE$ with ΔU representing the potential energy difference, nFE the electrical work (where n is the number of electrons involved in the reaction, F is Faraday's constant and E is the reversible potential of the cell) and with $T\Delta S$ representing the heat associated with a chemical reaction [8,9].

The above conditions result in $\Delta G = \Delta U - T\Delta S$, which yields $\Delta G = -nFE$. The ΔG is the change in free energy associated with the formation of product compounds from the reactants.

Using this relationship between the change in the Gibbs free energy and the reversible potential of the electrochemical reaction (*E*), the possibility of corrosion can be predicted [10,11].

E for a material is usually determined for a specific half cell versus a reference electrode such as a saturated calomel electrode (SCE) or a standard hydrogen electrode (SHE). Table 3.1 presents the electrochemical potential, *E*, vs SHE values for some selected metals [12].

Table 3.1 Standard electromotive force potentials for selected metals at 25°C vs. SHE [13].

Reaction	**Standard Potential, V**
$Au^{3+} + 3e^- = Au$	1.498
$2H_2O = O_2 + 4H^+ + 4e^-$	1.229
$Pt^{2+} + 2e^- = Pt$	1.2
$O_2 + 2H_2O + 4e^- = 4(OH^-)$	0.401
Cu2+ + 2e- = Cu	0.337
$2H^+ + 2e^- = H_2$	0
$Ni^{2+} + 2e^- = Ni$	-0.26
Cd^{2+} +2e- = Cd	-0.403
$Fe^{2+} + 2e^- = Fe$	-0.44
$Cr^{3+} + 3e^- = Cr$	-0.744
$Zn^{2+} + 2e^- = Zn$	-0.763
$Al^{3+} + 3e^- = Al$	-1.662

The anodic and cathodic reactions (i.e., production and consumption of electrons) occur at the same rate. Thus, the anodic current density (oxidation or corrosion rate) is equal to the cathodic current density (reduction rate). The current density is given by $i = i_o\, e^{(\phi/B)}$ where i_o is the exchange current density, ϕ is the overpotential or polarization, and *B* is the Tafel constant. The overpotential is the difference between the operating potential and the corrosion potential [14].

All conditions being equal, a greater current density indicates a higher corrosion rate for a material and it is said to be either anodic, when the anodic processes on the electrode are accelerated by changing the specimen potential in the positive (noble) direction or cathodic when the cathodic processes are accelerated by moving the potential in the negative (active) direction. Figure 3.1 shows a typical polarization curve for steel [15].

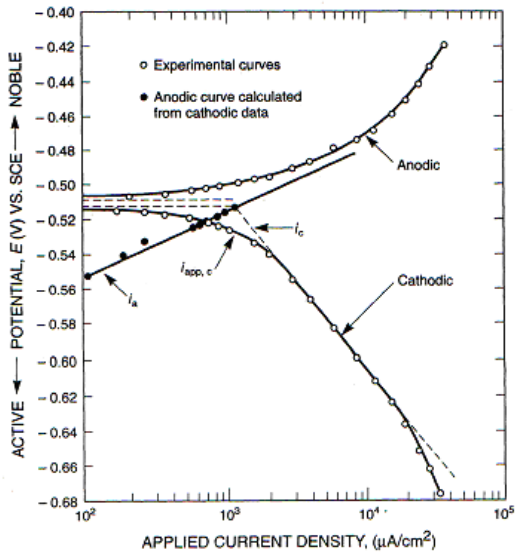

Figure 3.1 Experimental polarization curves for steel [8].

The Tafel extrapolation method is used to measure uniform corrosion rates. The Tafel slopes, being the slopes of the straight line portion of the semi-logarithmic polarization curve on both anodic and cathodic regions, are extrapolated until they intersect. Such crossing point is referred to as the corrosion rate or corrosion current density, i_{corr}.

3.2 Corrosion types and mechanisms

There are many types and causes of corrosion depending on particular tendencies to look upon the subject more broadly or narrowly. Most corrosion experts however, agree on the basic varieties of corrosion listed below:

Uniform corrosion: is defined as corrosion that is distributed more or less uniformly over the surface of the material. *Localized corrosion:* is often confined to a small area (pitting, grain boundary, etc.). *Galvanic corrosion:* results from electrically coupling two dissimilar materials,

where one acts as the anode and the other the cathode. *Velocity/Flow related attack:* arises when high surface liquid or particles velocities cause metal loss. *Environmentally assisted cracking:* encompasses a variety of cracking failure mechanisms that are enhance or altered by the environment.

3.3 Corrosion in steel

Carbon and low alloy steels have relatively low corrosion resistance and often require protective coatings, even in relatively noncorrosive environments [8]. Protection can be omitted only when carbon-steel surfaces are sheltered and dry.

Appreciable corrosion of iron or steel at near ambient temperature requires dissolved oxygen in neutral and alkaline solutions, like fresh water. On the other hand, a protective magnetite film is stable in the absence of dissolved oxygen. Any factors affecting dissolved oxygen thus affect the corrosion of steel proportionally. Solution agitation or stirring increases transport of dissolved oxygen and increases the corrosion rate. Dissolved solutes also decrease solubility of dissolved oxygen and the consequent corrosion rate [16].

The effect of pH on the corrosion of iron in aerated water is shown in Figure 3.2. In an acidic pH < 3, corrosion would be catastrophic. In the intermediate pH 4 through 10 ranges, a loose, porous, ferrous oxide deposit shelters the surface and maintains the pH at about 9.5 beneath the deposit, which increases the corrosion kinetics. At pH above 10, corrosion rate is slow, due to the formation of a passive ferric oxide film in the presence of dissolved oxygen. At pH above 14 the corrosion rates decreases [17].

The schematic effect of NaCl concentration on corrosion rate of iron in aerated room-temperature solutions is shown in Figure 3.3. The initial increase in corrosion rate is due to enhanced solution conductivity. Low conductivity allows only closely spaced anodes and cathodes, and anodic reaction products tend to limit cathodic oxygen reduction.

Seawater has a chloride content of about 3.5 wt.% that for low carbon steels gives a maximum corrosion rate higher than tap water. A NaCl solution of such concentration is sometimes used to simulate seawater in the laboratory. The bulk pH in seawater is commonly 8-

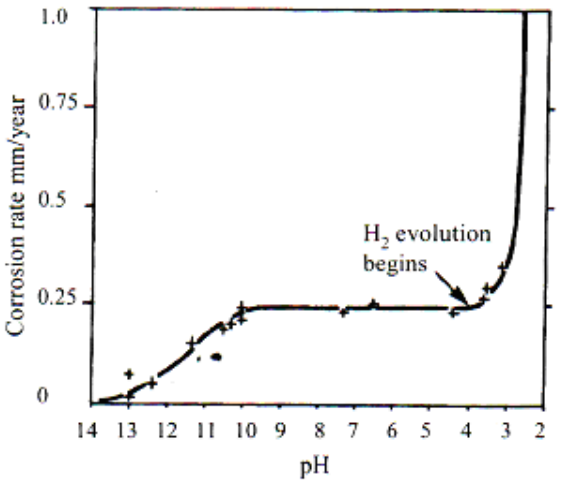

Figure 3.2 Effect of pH on corrosion of iron.

8.3, but due to cathodic production of OH^-, the pH value at the surface increases sufficiently for deposition of $CaCO_3$ and possibly to a smaller extent some $Mg(OH)_2$ together with iron hydroxide. The deposits form a surface layer that reduces oxygen diffusion so much that the average corrosion rate on steel in seawater is less than in fresh water.

Because the corrosion rate in seawater depends mostly on the supply of oxygen, it will be highest in the splash zone where a thin water film exists for a major proportion of the time, and where corrosion products frequently are washed away.

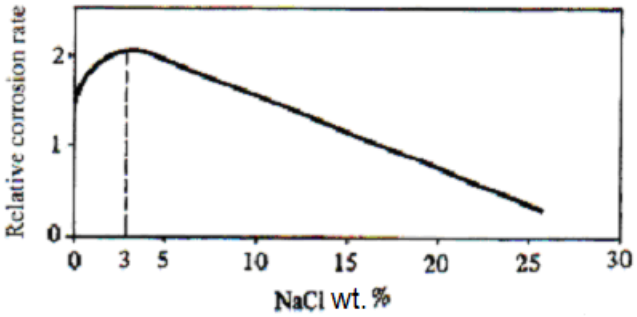

Figure 3.3 Effect of NaCl concentration on corrosion rate of steels in aerated solutions at room temperature.

3.4 Surface engineering

In many spheres of engineering it is recognized that, in order to obtain the optimum performance from a component or material, it is usually necessary to apply a surface treatment or coating. Thus, creating a composite system which has a performance that cannot be achieved by neither the coating nor the substrate alone [5,18].

Coatings play an important role in corrosion control. They are typically utilized in three different ways: **Barrier coatings,** which suppress both oxygen and ionic transmission to the cathode reaction to an extent that corrosion may be precluded. **Inhibitive/passivation coatings,** which decrease corrosion rates by chemically modifying the interfacial condition against the metal. **Cathodic coatings,** prevent galvanic corrosion by acting as anodes compared to the substrate which acts as a cathode. Metallic coatings are included in this category [13,19,20].

3.4.1 Metallic coatings

In most cases of corrosion protection by metallic coatings, the purpose is to protect unalloyed or low-alloy steel, but there also exist many cases of other metals to be protected this way. Metallic coatings can be divided in two groups, *cathodic* coatings, which are more noble than the substrate, and *anodic* or sacrificial coatings, which are less noble than the substrate, i.e. the coatings that have, respectively, a higher and a lower corrosion potential than the substrate in the environment in question [13].

The cathodic coatings will most often act by the barrier effect only, but for some combinations of substrate and environment the substrate can also be anodically protected (on uncovered spots). The anodic coatings will in addition to the barrier effect provide cathodic protection of possible spots or parts of the surface where the coating is imperfect and the substrate is exposed to the corrosive environment. For such reason, anodic coats sometimes are referred to as “sacrificial” coats [21,22].

The normal major difference between a cathodic and an anodic coating is just the behavior at such a defect. This is illustrated in Figure 3.4. In the case of cathodic coatings (a) the substrate is subject to galvanic corrosion in the coating defect. The corrosion may be rather

intensive because the area ratio between the cathodic coating and the anodic spot of bare substrate usually is very high. In the other case (b), only a cathodic reaction occurs on the bare substrate (it is protected cathodically), while the coating is subjected to a corresponding galvanic corrosion distributed over a larger surface area [13,23].

In relation to steel, Ag, Ni, Cr and Pb are cathodic, while Zn and Cd are anodic in most environments.

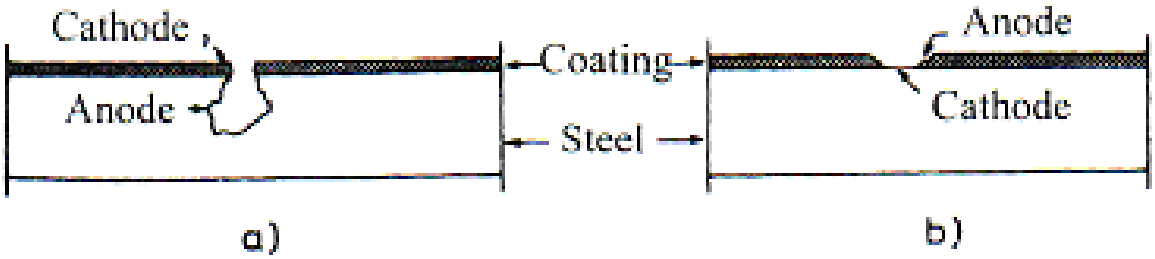

Figure 3.4 Localization of corrosion at a defect in a metal coating on steel. a) Cathodic coatings and b) anodic coatings.

Silver is used as a coating metal for decoration purposes; furthermore its chemical and electrical properties are utilized, respectively, in various equipment and environments in the process industry and in electrical contacts and other small components in electronic equipment [5,7].

Nickel has often been used for preventing corrosion and for providing a nice surface on steel parts in contact with ordinary atmosphere. Nickel and its alloys are the most corrosion-resistant engineering alloys, thus it is an important group for applications in aggressive environments and for purposes where long lifetime is required.

In order to make the surface brighter and more corrosion resistant the nickel plate is covered by a thin coating of chromium. Depending on the service conditions and the type of nickel and chromium coating, the recommended thickness of nickel can vary from 5 to 40 μm and of chromium from 0.3 to 0.8 μm. The chromium coating has a large number of micro pores or micro cracks, which is advantageous because they make the corrosion of the underlying nickel well distributed and shallow. The chromium layer is usually deposited on top of a thin layer of bright nickel, which is anodic in relation to a thicker basic layer of nickel. Because of its less noble

nature, the bright nickel layer gives a certain cathodic protection effect on the basic layer in existing pores [13].

For industrial use, Ni coatings are applied as pure Ni if the substrate is not steel. Such coatings are most often around 25-250 μm and are most suitable for environments that tend to cause general corrosion with reaction products of low solubility (environments without chlorides). However, it is also stated that nickel performs well in seawater provided that the flow rate is high. Furthermore, the experience with nickel in various alkalis, neutral and alkaline salts and organic chemicals is good. Electrochemical deposition (electroplating) has traditionally been the dominant technique for application of nickel coatings [7,13].

Nickel coatings can increase the resistance to corrosion fatigue, but stresses set up by the coating may reduce the pure mechanical fatigue strength of the base material. The effect can be counteracted by compression stresses in the coating, which can prevent cracks in the coating propagating into the base material.

Lead is particularly suitable in coatings exposed to dilute sulfuric acid and industrial atmospheres.

Tin shows rather complicated corrosion properties in contact with steel. In the atmosphere and in solutions of natural inorganic salts, Sn is cathodic in relation to Fe. In contact with fruit juice, milk and alkaline solutions, tin is anodic.

Zinc. The Pourbaix diagram for zinc is shown in Figure 3.5. The boundaries of passivity region shown by solid lines are valid for water without CO_2. For pH $<$ 8-9, the following reactions occur: $Zn \rightarrow Zn^{+2} + 2e^-$ as the anodic reaction and both $2H^+ + 2e^- \rightarrow H_2$ and $O_2 + 2H_2O + 4e^- \rightarrow 4OH^-$ as the cathodic reaction [5,7,13].

The equilibrium potentials of the three reactions as functions of pH are drawn in the diagram. For pH values between 8.5 and 11, zinc is passivated by formation of $Zn(OH)_2$. When CO_2 is dissolved in the corrosive medium the passive region is enlarged so that it reaches from pH = 6 to pH = 11 (dashed lines). The reason for this is the formation of a protective film of alkaline zinc carbonate. The effect of this film is strong in rural atmospheres, in mildly aggressive

city atmospheres and in neutral and slightly acidic rain water. Also the calcium content in hard waters leads to deposits that prevent corrosion. Conversely, in various salt solutions the

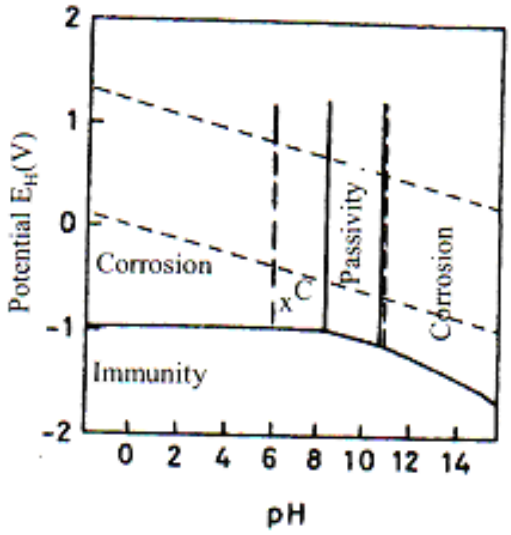

Figure 3.5 Pourbaix diagram for Zn in water at 25°C. The corrosion potential in seawater is marked with “C” [13].

formation of soluble corrosion products may counteract the passivation process. Chlorides act in this way, but in marine atmospheres and seawater, the detrimental effect of chlorides at least partly balanced by protective calcareous deposits. Corrosion of zinc in seawater is therefore mainly under cathodic control, which is also indicated by the level of corrosion potential (marked C in the diagram in Figure 3.5) [25,26].

Another important factor is the temperature. The corrosion rate at 70°C may be 50 times that at 20°C. Above 60-70 °C, zinc is cathodic in relation to iron and carbon steel.

In spite of its electronegative character, zinc corrodes relatively slowly when separated from other metallic materials. The reasons are that $2H^+ + 2e^- \rightarrow H_2$ does not go fast on Zn, and that, under atmospheric conditions, a protective layer of carbonate is formed. As a coating on a more electropositive material such as carbon steel (at $t < 60$°C), the corrosion rate of zinc is increased near the bare steel region. The potential at these places will increase to some extent compared with the normal potential on zinc, but it will remain below a practical limit for corrosion of steel. For larger uncovered regions, the following should be noted: with increasing distance

from the zinc, the potential of the steel surface increases, and at a certain distance significant corrosion of steel will occur. This critical distance increases with increasing conductivity of the liquid and its corrosivity versus zinc. However, at the same time as an increased area of bare steel can be protected, the corrosion rate of zinc may be so high that protection of steel with zinc is not an economic method. In such cases, coating the steel with aluminum may be a better alternative, but possible bare steel regions must then be kept small [27].

Cadmium has been a very useful coating material, but because of its toxic nature the numbers of applications has been reduced during recent decades [7,8].

3.4.1.1 Zn-Ni alloy coatings

Over the last few years, many efforts have been devoted to developing electro deposition systems for Zn–Ni alloy coatings, which are promising because of their high corrosion resistance and good mechanical properties. They also offer an important alternative to toxic Cd coatings. Apart from chemical composition, the corrosion resistance of Zn–Ni coatings depends mainly on their microstructure, phase composition and structural parameters (texture and lattice imperfections) [28].

An increase in the nickel composition would lead to more positive open-circuit potential of the alloy, Figure 3.6, which in turn will reduce the driving force for galvanic corrosion [2]. Additions of 9.5 to 20% Ni in Zn coats reportedly gives dramatic improvement in corrosion resistance in seawater and humid atmosphere. A Ni content of 9.5 to 12.5% yields a ductile coating with low internal stress.

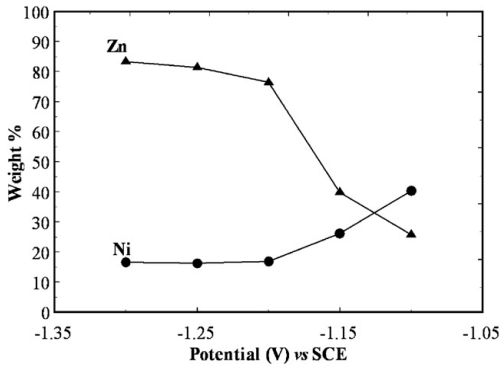

Figure 3.6 Effect of applied potential on the composition of Zn–Ni deposits [2].

3.4.2 Traditional coating methods

It is important to recognize that the selection criteria for choosing one surfacing technique over another are complex and a number of issues need to be addressed including:
1- The coating should not impair the properties of the bulk material. 2- The deposition process must be capable of coating the components, in terms of both size and shape. 3-The technique must be able to produce the desired coating thickness. 4- It must be cost-effective [1,13].

Electrolytic plating. Compared with other coating methods, electrolytic deposition is favored by low process temperatures. Hence, any heat effect, which might cause changes in structure, shape and mechanical properties of the substrate, is avoided. As for other methods, both local and overall geometry of the surface to be coated must be carefully considered as part of the design work. Cavities, where air or liquid may be enclosed, cannot be accepted, and sharp corners should be avoided. Since the coating usually is thin (5-40 μm), factors such as roughness and porosity in the substrate may cause problems that do not exist for the methods where thicker coatings are common.

For electrolytic deposition of zinc, it is easier to control the coating thickness than it is for hot dipping and thermal spraying. Any alloy element which promotes brittleness, can not be included in electroplated Zn coatings, i.e. the latter is more ductile. But the lifetime of zinc coatings is nearly proportional to the thickness, independent of coating method, and this limits the number of applications of electroplated Zn.

Hot dipping: Zinc, tin and tin/lead coatings are commonly applied by hot dipping, i.e. dipping the object to be coated in molten coating metal. Aluminizing by this method is less widespread, because Al makes the process more difficult to operate.

Hot-dip galvanizing is the most economical method in cases where a relatively thick Zn coating (up to 100-200 μm) is needed or desirable on components that can be placed in a bath without much difficulty. The normal temperature of the galvanizing bath is 445-465°C.

Thermal spraying: Most metals can be thermally sprayed. For corrosion protection of steel in waters and the atmosphere, aluminum and zinc are of particular importance. These

coatings are usually from 100 to 300 μm thick. Other materials such as stainless steel are also sprayed with good results and have important application.

The special advantages of thermal spraying compared with other coating methods are just that thicker coatings can be applied, and particularly that the spraying equipment is portable, so that the coating work can be carried out almost anywhere. The drawbacks of thermal spraying are considered to be relatively high cost, relatively low adhesion between substrate and coating, high porosity in the coating and rough surface. In order to obtain a good result with thermal spraying it is quite necessary that the base material is clean, dry and rough all over prior to spraying [13,29].

Conversion coating: are coatings for metals where the part surface is converted into the coating with a chemical or electro-chemical process. Liquids such as zinc acid orthophosphate solutions form an adherent phosphate layer on the metal surface. The phosphate layer is, however, rather porous and is more often used to improve paint adherence. Stable, adherent, nonporous, non-conductive ox-delayers form on the surface of aluminum, chromium and stainless steel. These oxides exclude the electrolyte and prevent the formation of galvanic cells.

They are used for corrosion protection, increased surface hardness, to add decorative color and as paint primers. Conversion coatings may be very thin, on the order of 0.00001". Thick coatings, up to 0.002", are usually built up on aluminum alloys, either by anodizing or chromate conversion [29].

3.4.3 Electrolytic plasma processing (EPP)

The EPP technique involves electrolysis and electrical discharge phenomena and it is environmentally friendly surface engineering technology. Electrolytic plasma/material surface interactions during processing can be used for cleaning of metal surfaces, formation of diffusion layers and/or deposition of metal, ceramic and composite coatings. The deposition rates typically are more than 10 μm per minute [30].

3.4.3.1. Process description

Electrolytic plasma processing involves two characteristic phenomena (i) electrolysis of a liquid environment by application of different electrical potentials between the work piece material and a counter-electrode; and (ii) the production of an electrical discharge at, or in the vicinity of, the work piece surface. Although the discharge phenomena associated with electrolysis were discovered more than a century ago, their importance as an emerging surface engineering process were realized only very recently. A typical electrode current–voltage characteristic curve of the electrolytic cathodic process is shown in Fig. 3.7. The normal glow discharge zone U_2–$U_{2'}$–U_3 is usually selected as the work region, where the electrode current decreases but plasma intensity increases when the electrode voltage increases from U_2 to $U_{2'}$. The samples (as a cathode) can be either immersed in the electrolyte, Fig. 3.7(a), or dripped with electrolyte, Figure 3.7(b). However, the corresponding slope of the electrode current–voltage curve in the U_2–$U_{2'}$ segment is different in these two cases [4,31].

For the configuration shown in Fig. 3.7(a) (i.e. the work piece is immersed in the electrolyte), the current sharply drops from the highest point to the lowest point when the electrode voltage increases from U_2 to $U_{2'}$. For the configuration in Fig. 3.7(b) (i.e., in this case, the electrolyte drips down to the work piece through small diameter holes on the cathodic electrode plate), the slope of the U_2–$U_{2'}$ line (i.e. current reduction rate) is much smaller than that of Figure 3.7(a). It is found that the plasma intensity increases when electrode voltage increases, and when $U_{2'}$ is reached, a continuous envelope is formed on the sample surface, which results in rapid increase of the surface temperature with increasing electrode voltage. The normal operation voltage in this work is within U_2–$U_{2'}$. Although there is heating of the substrate due to plasma action, the bulk substrate temperature remains relatively low (less than 200–300℃) due to the simultaneous cooling action by the electrolyte solution. The local surface temperature adjacent to plasma bubbles, however, is very high, around 1500 °C, which is critical to cleaning mill-scale and enhancing the metallurgical adherence of the coating [4].

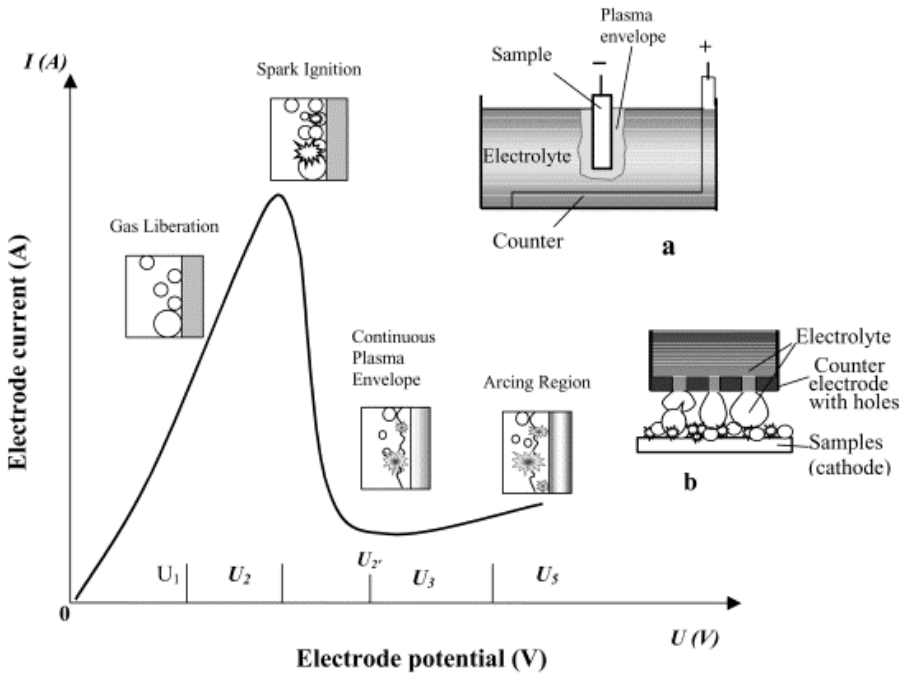

Figure 3.7 Current–voltage dependence in electrolytic plasma discharge.

There appears to be several distinct physical processes involved in cleaning and subsequent coating using EPP. While the electrolyte flows through the perforated anode onto the work piece (cathode), Figure 3.8, a potential is applied across the electrode gap and sets up a strong electric field.

The hydrogen evolution reaction begins to occur at the surface of the work piece, creating fine hydrogen bubbles. A strong electrical potential is established on the bubble adjacent to the work piece surface, and hydrogen plasma is thus generated in a thin layer, just above the steel surface.

Metal cations present in the electrolyte film begin to migrate toward the steel surface, but the large majority of these ions are attached to the hydrogen bubbles. These ions are either original additions to the electrolyte or are generated from the anode metal by electrolytic decomposition.

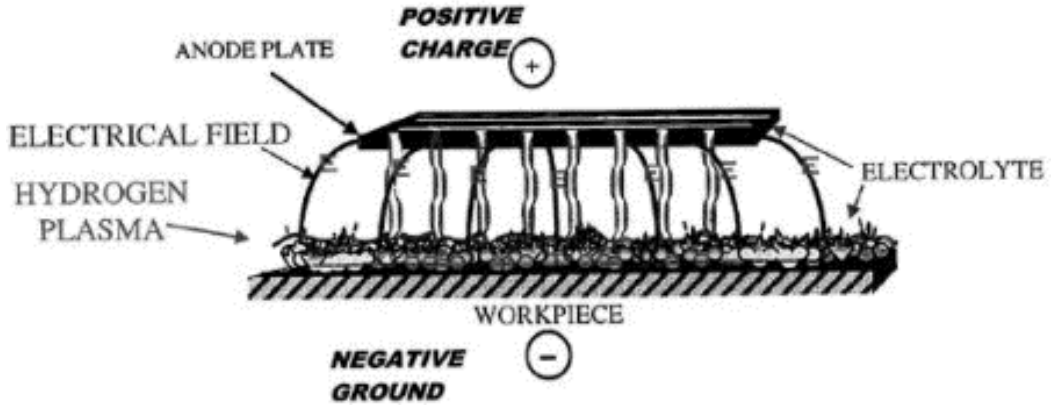

Figure 3.8 Schematic illustration of the electrolytic plasma process.

In particular, in the case of cleaning, the cations may be sodium (i.e. sodium carbonate solution) which will participate in the process but ultimately remain in solution. The ions due to adsorption gradually concentrate on the hydrogen bubble surface and the bubble is thus converted into a small capacitor. The electrical field between the positive ions at the bubble surface and the negatively charged steel surface ionizes the hydrogen gas in the bubble, resulting in high temperature plasma. This occurs quickly once hydrogen starts forming. The lifespan of the average hydrogen bubble is less than 1 ms and the plasma exists for 1–10 μs. The plasma is continuously forming at this high rate over the entire steel surface. The nature of the plasma bulb generation and extinction results in local surface melting and also creates forceful pressure disruptions at the surface associated with bubble collapsing and shock wave production. The net effect of these processes is the removal and/or reduction of the milling-scale at the steel surface and the formation of circular wavelets and spheroids. Also, the freezing that follows local melting causes a quenching effect that may result in ultra fine grained (or even amorphous) structures, as shown later in this work.

In the coating process, some metal ions may find their way to the steel surface by diffusion through the electrolyte but the predominant modes of transport are ion acceleration through the plasma and ion bubble adsorption transport where ions are carried to the steel surface by riding the surface of the hydrogen bubble as it collapses. Both of the latter processes eliminate the boundary layer diffusion and result in high deposition rates [2].

CHAPTER 4

EXPERIMENTAL PROCEDURE

4.1 Material processing

Various deposition experiments were conducted at CAP Technologies (Baton Rouge, LA) by EPP in order to select desirable Zn-Ni coatings as potential replacement of Cd coatings. All depositions were conducted on 4340 steel that was first cleaned by EPP. Typical cleaning conditions involved: voltage 170-200 V, current 0.23-0.45 A/cm^2 and 14% $NaHCO_3$ electrolyte at 75 °C. The processing time was 15 seconds. The first series of deposition experiments (Series 1) were conducted to investigate the effect of Ni content on the electrochemical properties of the coating. The deposition parameters employed are shown in Table 4.1. The Ni content in the coatings was varied by controlling the content of the Ni salt in the electrolyte.

Table 4.1 Deposition parameters of the Zn-Ni coatings for Series 1. Voltage was set at 190 V for all cases.

Coating	%Ni salt in electrolyte*	pH	Conductivity (ms @ °C)	Electrolyte T (°C)	Current (A)	Dwell time per coat (s)
1A	6	4.4	42 @ 65	65	50	30
1B	14	4.2	43 @ 72	72	50	30
1C	26	4	49 @ 70	70	70	4.7
1D	30	4.3	37 @ 78	78	55	9.4
1E	50	4.5	39 @ 77	77	55	9.4

* Electrolyte: $ZnSO_4.7H_2O$ and $NiSO_4.6H_2O$

Based on the results from Series 1 experiments, Series 2 coatings were deposited using lower Ni salt content in the electrolyte. Table 4.2 presents the Series 2 parameters that were selected in order to reduce the Ni content of the coatings (< 25 wt% Ni). Only Zn-Ni coatings with < 25 wt% Ni have the potential to act as sacrificial coatings in conjunction with steel [45]. It is important to mention, that the Ni content in the deposited coating depends not only on the Zn/Ni ratio of the salt dissolved in the electrolyte, but on the deposition parameters used and the Ni and

Zn deposition characteristics. Another issue explored here is the effect of conversion coatings. It is a common engineering practice to apply a conversion coating on electroplated Cd coatings to improve their corrosion resistance [30]. Thus, the two most common types of conversion coatings were applied over some Zn-Ni coatings to study their effect. These conversion coatings were Dipsol and Metalast, which are both Chromate based.

Table 4.2 Deposition parameters of the Zn-Ni for Series 2. Dwell time per coating was set at 20 seconds in all cases.

Coating	% Ni salt in electrolyte*	Conversion Coating	pH	Conductivity (ms @ °C)	Electrolyte T (°C)	Voltage (V)	Current (A)
2A	18	**Dipsol	2.7	32 @ 85	85	190	45
2B	18	***Metalast	2.8	29 @ 84	84	190	50
2C	16	NA	2.9	36 @ 85	85	195	55
2D	16	Dipsol	2.8	37 @ 85	77	195	55

* Electrolyte: $ZnSO_4.7H_2O$ and $NiSO_4.6H_2O$
** Commercial name: IZ 258 (Hexavalent Cr chromate based)
*** Commercial name:TCP-HF (Trivalent Cr chromate based)
NA: Not Applied

Series 3 experiments were conducted as a final step to deposit lower Ni content coatings and to confirm their electrochemical properties. Table 4.3 presents the deposition parameters.

Table 4.3 Deposition parameters of the Zn-Ni for Series 3. Dwell timer per coating and current were set as 60 seconds and 20 A for all cases.

Coating	% Ni salt in electrolyte*	Conversion Coating	pH	Conductivity (mS @ °C)	Electrolyte T (°C)	Voltage (V)
3A	12	**Dipsol	3.9	36 @ 85	85	195
3B	12	Dipsol	3.8	36 @ 85	85	195
3C	12	***Metalast	3.7	40 @ 85	85	195
3D	12	NA	3.9	39 @ 85	85	195
3E	12	NA	3.9	39 @ 85	85	195

* Electrolyte: $ZnSO_4.7H_2O$ and $NiSO_4.6H_2O$
** Commercial name: IZ 258 ((Hexavalent Cr chromate based)
***Commercial name: TCP-HF (Trivalent Cr chromate based)
NA: Not Applied

4.2 Sample preparation

Following coating deposition, cross sectional specimens were prepared by first sectioning using a LECO VC-50 cutting machine with a diamond tip blade at a speed of no less than 6 cm/s. Subsequently, metallographic specimens were prepared by mounting in epoxy resign, grinding and fine polishing with 0.5 μm diamond paste as the final step in order to be studied by SEM/EDS.

4.3 Scanning electron microscopy characterization

Scanning electron microscopy (SEM) (Zeiss Supra 55 VP with Genesis 4000 EDAX) at a typical acceleration voltage of 20 keV, was used to characterize the coating surface morphology and the cross sectional samples. The substrate/coating interface was examined in order to determine coating adhesion, density and other characteristics. For Series 2 and 3 depositions only the surface morphology was studied.

The chemical composition of the coatings for all the samples was determined by X-ray energy dispersive spectroscopy (EDS). On a first approach, all the major elements present in the coatings were determined. Then, in order to determine the zinc and nickel content present in the different phases, spot or small area analysis was performed on several specific areas.

4.4 Phase structure characterization

The phase structure of the coatings was studied by X-ray diffraction (XRD) using a Cu K_α radiation source (λ = 1.542 Å) with an accelerating voltage and filament current of 40 kV and 30 mA, respectively. XRD patterns were only taken from all Series 1 coatings and phase analysis was conducted to study possible Zn-Ni phases present in the coatings.

4.5 Electrochemical characterization

Electrochemical characterization was performed on all samples. Corrosion potential (E_{corr}) and potentiodynamic experiments were conducted to characterize the corrosion behavior of the EPP-coated specimens. A three electrode electrochemical cell was utilized for these experiments filled with 0.5 L of electrolyte. A schematic description is given in Figure 4.1.

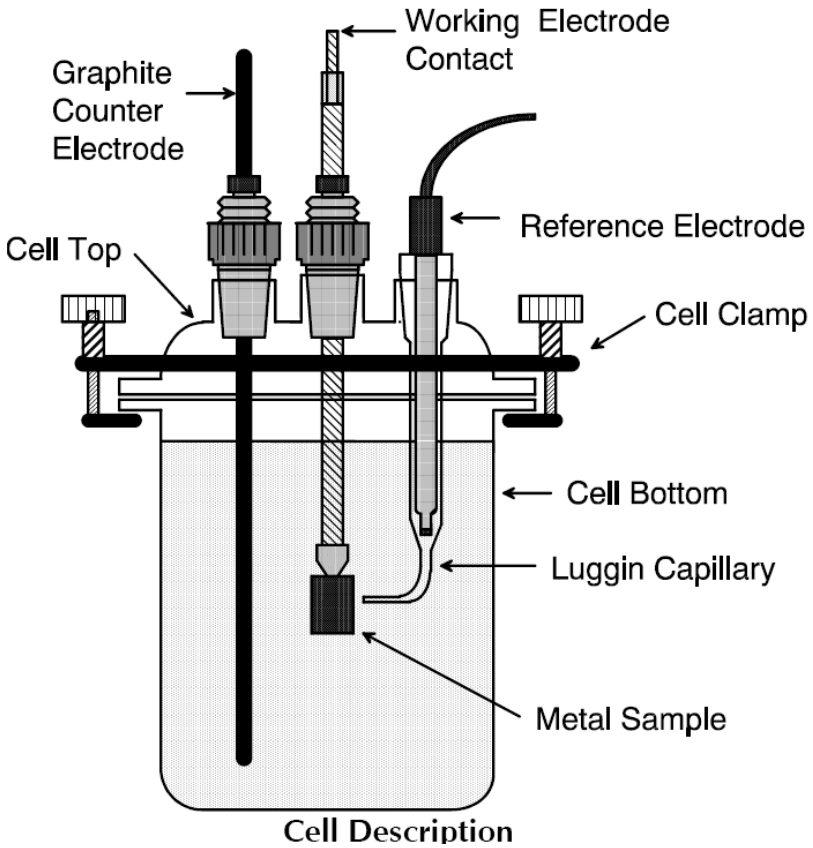

Figure 4.1 Schematic representation of the corrosion cell used for testing. All its prominent parts are shown.

A threaded road was attached to samples by drilling and taping a 3-48NC tap. Subsequently an insulating laquer (Microstop) was used to seal the specimen preventing contact with the electrolyte.

Corrosion potential measurements and potentiodynamic tests were conducted in tap water and 3.5% NaCl solution under aerated (laboratory air) and deaerated conditions. Tap water was selected to simulate effects by humidity or rain whereas the NaCl solution provided a more aggressive environment. Deaerated conditions were obtained by sealing the experimental flask and purging Ar in the electrolyte. In these experiments the electrolyte was purged with Ar for 15 min prior testing. In the corrosion potential experiments, E_{corr} was measured versus time until the potential was stabilized. In the potentiodynamic experiments, the potential was increased in steps from 200 mV below E_{corr} to 800 mV above E_{corr} at a rate of 1 mV/sec while the corrosion current

was measured. Corrosion rates were calculated using Tafel extrapolation. All corrosion potentials were measured with respect to a saturated calomel electrode (SCE).

After testing, the specimens were rinsed in distilled water, dried in compressed air and immediately placed in a desiccator for avoiding media interaction with the samples. Finally, using an outside source, ASTM B117 salt fog testing was performed on Series 3 coatings to assess the conversion coating corrosion protection properties. This is a typical test conducted by the aerospace industry to characterize performance of coatings.

CHAPTER 5

RESULTS AND DISCUSSION

5.1 Characterization of Series 1 coatings

5.1.1 Morphology and composition

SEM examinations (performed by Dr. S. You) showed that all Zn-Ni coatings exhibited similar morphology. All coatings were found to contain a mixture of a nodular-type phase and a flake-type phase. Typical surface morphologies are shown in Figures 5.1-5.5.

Compositional analysis from the surface of the coatings was conducted by EDS in conjunction with SEM. Typical EDS spectra for Series 1 coatings 1B, 1D and 1E are shown in Figures 5.6(a), (b) and (c), respectively.

Table 5.1 summarizes the chemical composition of the coatings of Series 1. The values shown are the average of at least three measurements. Chemical composition based only on Zn and Ni was also calculated to facilitate the analysis. It is evident that the Ni content increases from about 15 to 30 wt.% throughout the five coatings. The analysis shows the presence of carbon, oxygen and traces of sulfur in all coatings. Such elements are typically present in all coatings produced by EPP.

The influence of nickel salt concentration in the electrolyte on the Ni content in the coatings is shown in Figure 5.7. The solid line shows the composition reference line (CRL) corresponding to a coating composition that is proportional to the zinc and nickel salt content in the electrolyte. According to Brenner's classification [32], when the content of Ni in the coatings is located above the CRL line, it can be said that this is a 'normal co-deposition'. When the Ni content in the coatings is located below this line, it can be said that this is an 'anomalous co-deposition.

Table 5.1 Chemical composition of Zn-Ni coatings obtained by EDS.

Element	Ni		Zn		O		C		Fe		S		*Ni/Zn	
Coating	wt%	at %	wt%	at %	wt%	at %	wt%	at %	wt%	at %	wt.%	at.%	wt.%	at.%
1A	9.23	4.23	39.6	16.14	2.23	3.73	29.9	66.38	18.8	9.01	0.24	0.15	15/85	20.8/79.2
1B	12.94	8.54	67.6	40.66	6.04	14.64	11.22	34.64	2.19	1.52	0.52	0.60	18/82	17.6/82.4
1C	16.11	8.65	54.1	26.09	22.09	43.52	7.68	20.18	-	-	1.12	1.57	20/80	24.9/75.1
1D	16.88	12.72	66.49	44.98	5.65	15.61	6.05	22.26	4.04	3.2	0.96	1.24	24/76	22/88
1E	20.43	11.67	48.9	25.09	8.23	17.25	14.62	40.83	6.78	4.07	0.82	1.08	30/70	31.7/68.3

* Composition based only on Zn and Ni

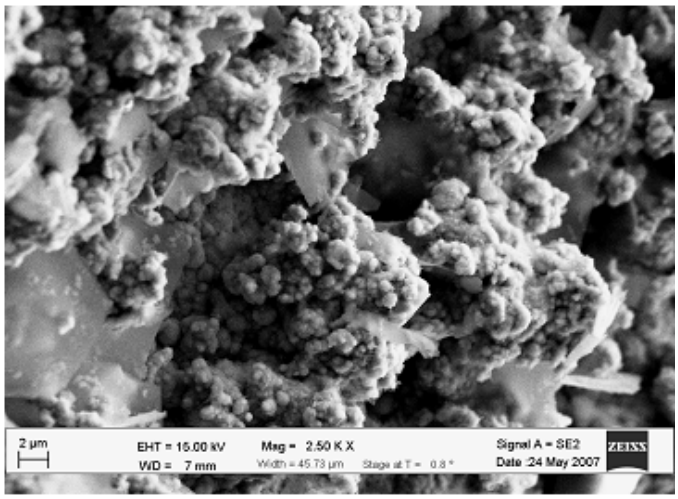

(a)

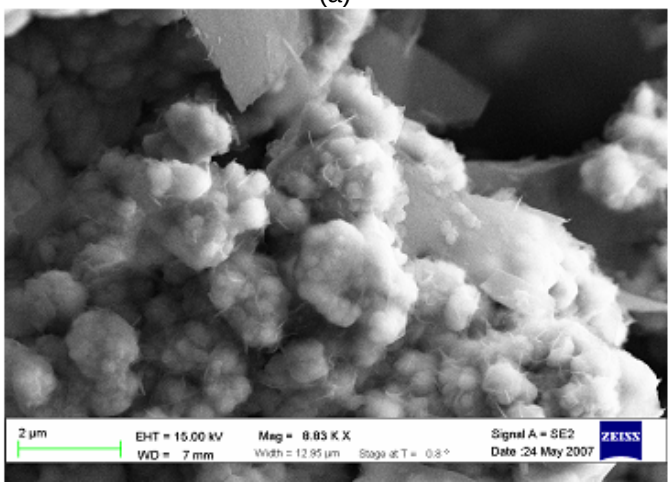

(b)

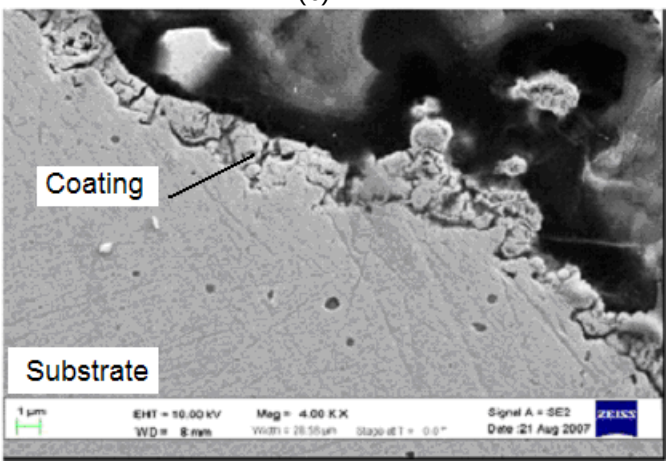

(c)

Figure 5.1 SEM micrographs of coating 1A: (a) overall surface morphology, (b) high magnification of (a), and (c) coating cross section.

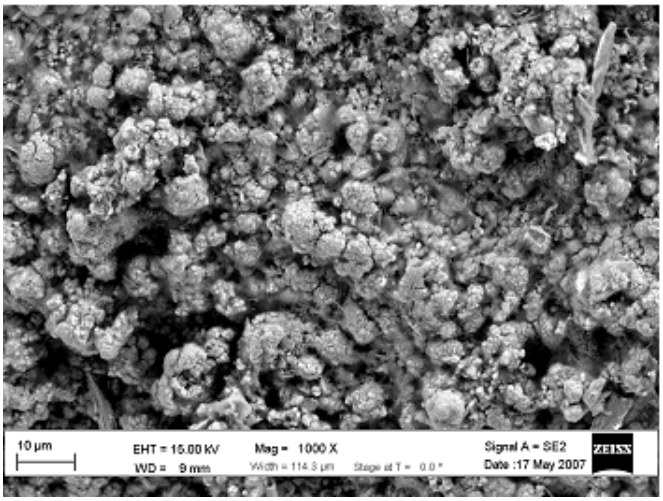

(a)

(b)

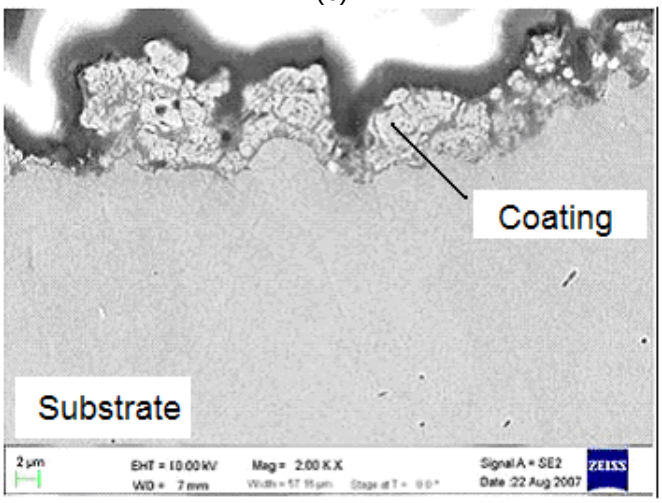

(c)

Figure 5.2 SEM micrographs of coating 1B: (a) overall surface morphology, (b) high magnification of (a), and (c) coating cross section.

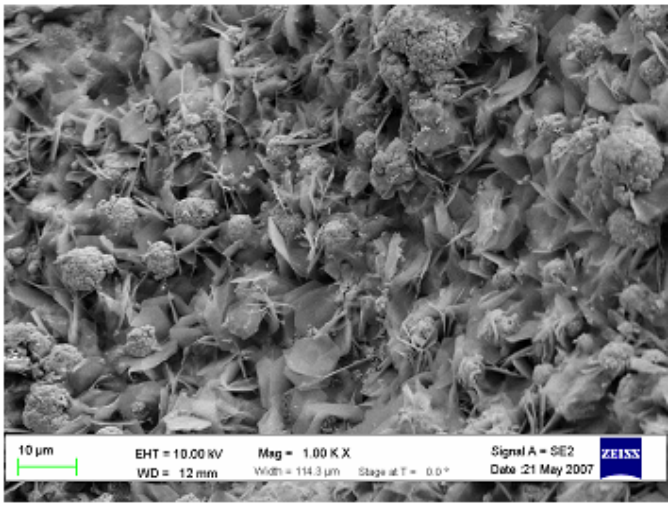

(a)

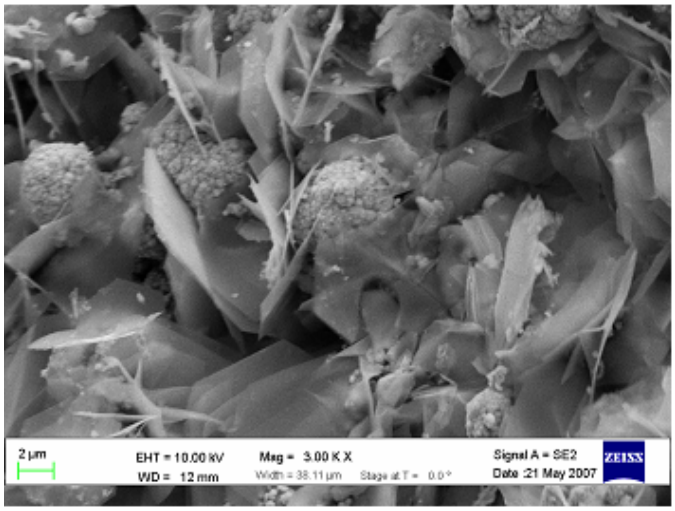

(b)

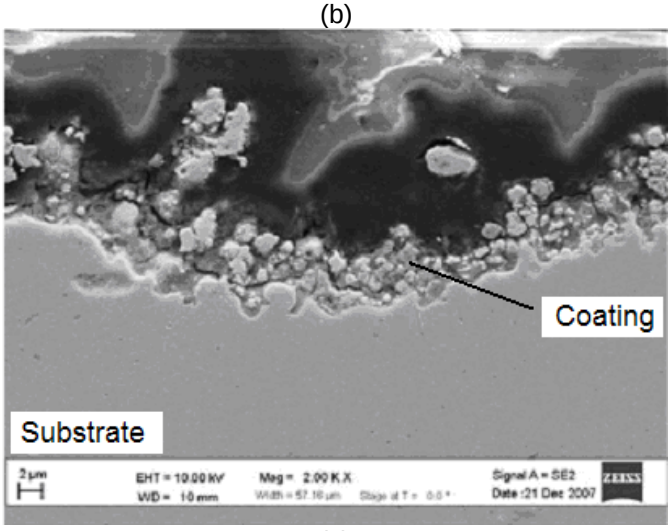

(c)

Figure 5.3 SEM micrographs of coating 1C: (a) overall surface morphology, (b) high magnification of (a), and (c) coating cross section.

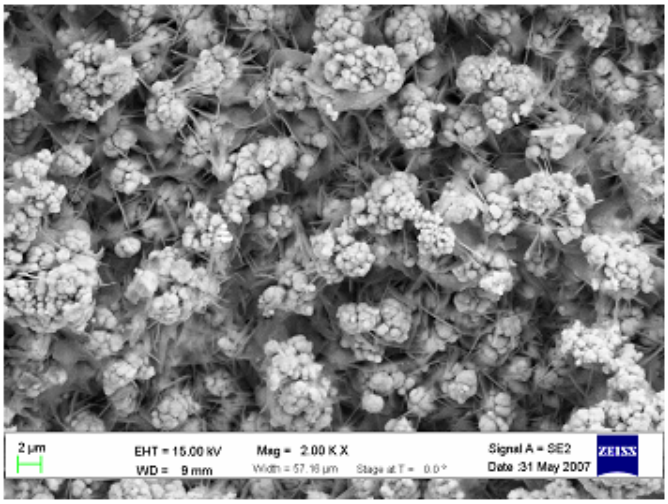

(a)

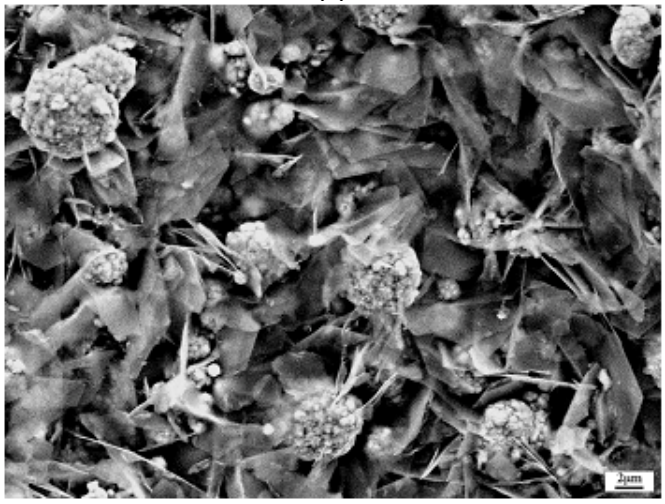

(b)

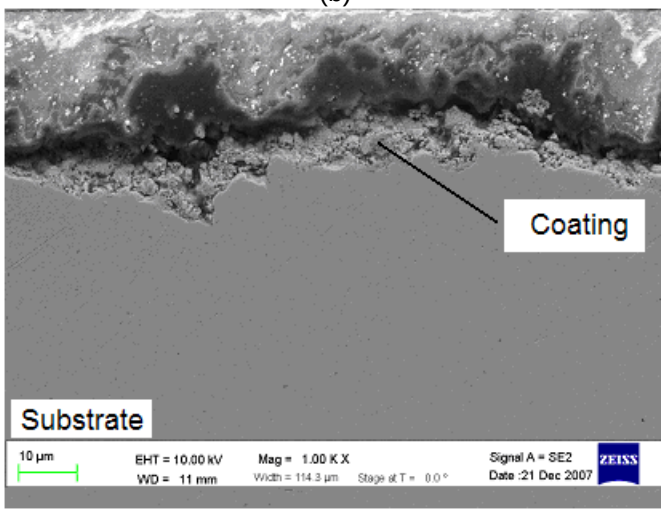

(c)

Figure 5.4 SEM micrographs of coating 1D: (a) overall surface morphology, (b) high magnification of (a), and (c) coating cross section.

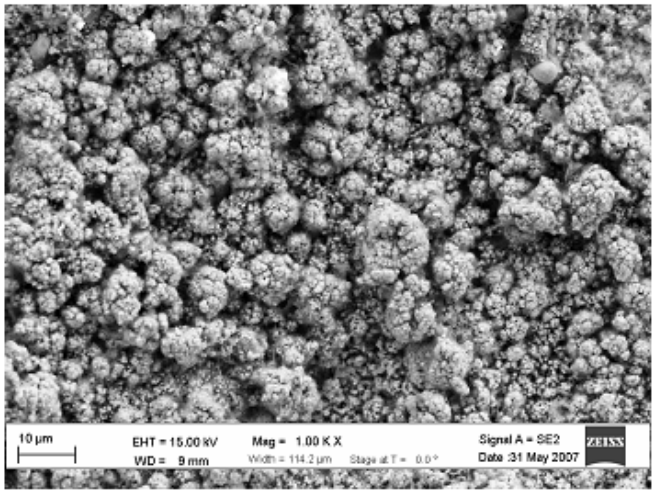

(a)

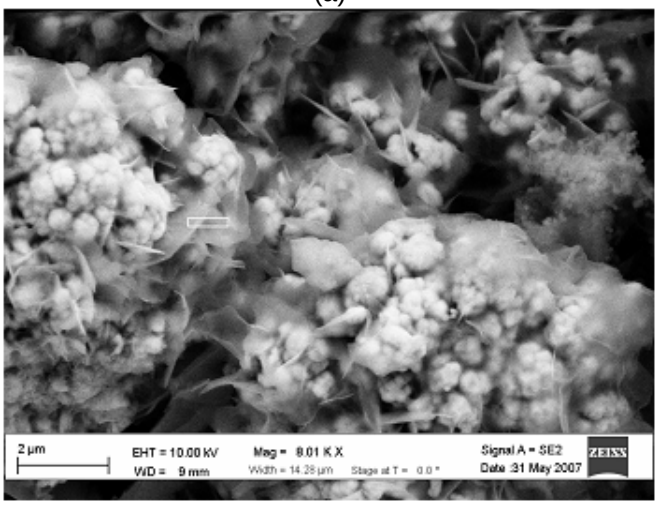

(b)

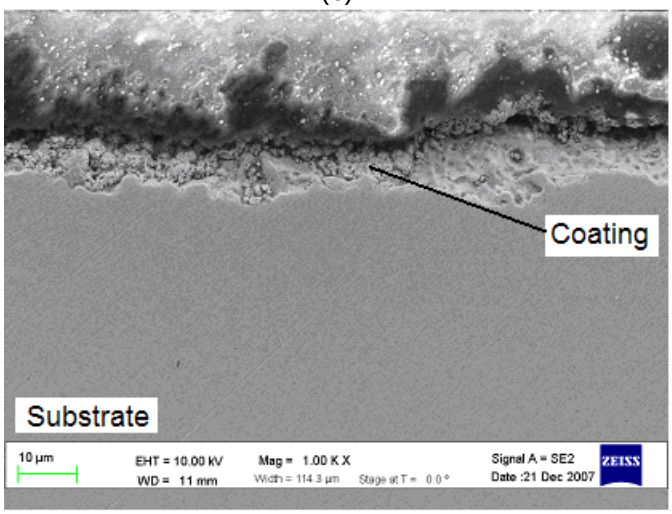

(c)

Figure 5.5 SEM micrographs of coating 1E: (a) overall surface morphology, (b) high magnification of (a), and (c) coating cross section.

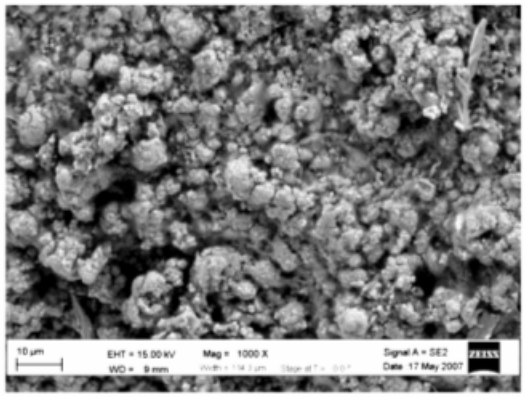

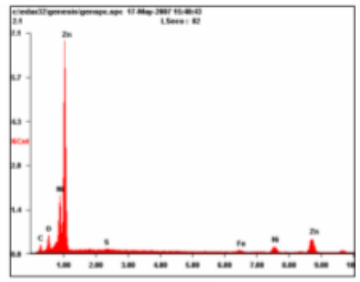

Element	Wt %	At %
C K	10.74	34.64
O K	06.04	14.64
S K	00.50	00.60
FeK	02.19	01.52
NiK	12.94	08.54
ZnK	67.59	40.06

(a)

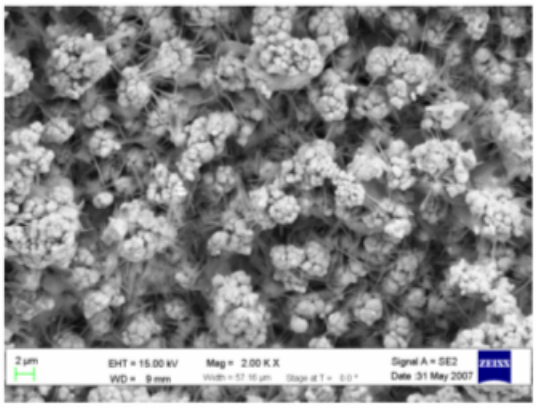

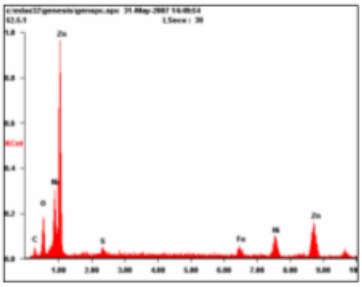

Element	Wt %	At %
C K	06.05	22.26
O K	05.65	15.61
S K	00.90	01.24
FeK	04.04	03.20
NiK	16.88	12.72
ZnK	66.49	44.98

(b)

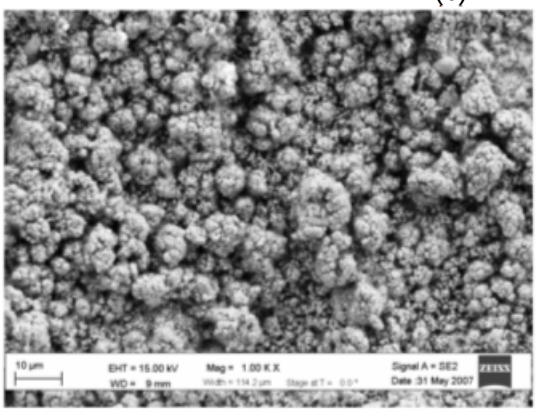

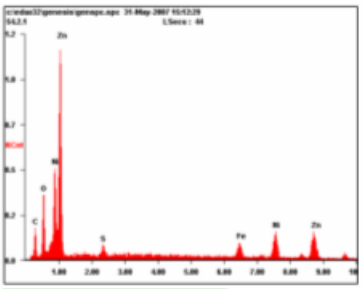

Element	Wt %	At %
C K	14.62	40.83
O K	08.23	17.25
S K	01.04	01.08
FeK	06.78	04.07
NiK	20.43	11.67
ZnK	48.90	25.09

(c)

Figure 5.6 Typical overall EDS spectra of coatings: (a) 1B, (b) 1D, and (c) 1E.

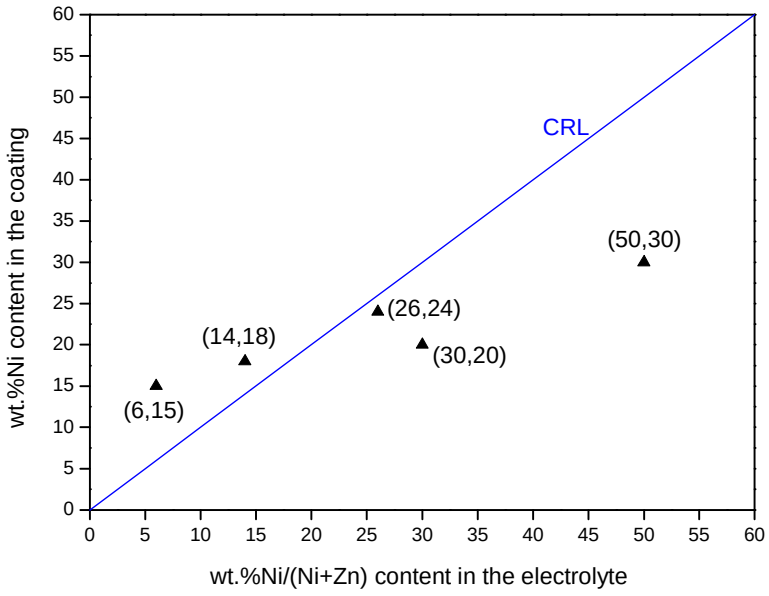

Figure 5.7 Variation of Ni content in the coatings versus the Ni/(Ni+Zn) ratio in the electrolyte.

From this study it can be seen that the Ni content in the coatings from the electrolyte with nickel salt concentration of 6 wt.% and 14 wt.% was above the CRL line, while that from the electrolyte nickel salt concentration of 26 wt.%, 30 wt.% and 50 wt.% was below the CRL line. Thus, the present results show that Zn deposition is favored in EPP coatings from electrolytes with high Ni salt content. A similar potential-dependent trend has been observed in Ni electroplating [4].

The surface of the Zn-Ni coating 1A and 1B (15 and 18 wt.% Ni), respectively, showed nonuniform agglomerations of nodular grains with fissures. A small amount of flake phase could be observed among those nodular grains using high magnification, Figures 5.1(b) and 5.2(b). Coating 1B contained less flake phase than the rest of the coatings from Series 1.

Figures 5.3 and 5.4 show the surface of the coatings 1C and 1D (20 and 24 wt.% Ni), respectively. These surfaces presented higher quantity of a relatively uniform flake phase, which formed around the nodular grains. This induced the formation of a lesser tightly packed surface morphology compared to that observed for coatings 1A and 1B. Coating 1D presented an abundant and larger flake grains than any other coating of Series 1.

When the Ni content in the coating reached 30 wt.% (coating 1E), the size of the agglomerate of nodular grains was much larger than that of the coating with 24 wt.% Ni. The flake grains which were finer tended to be needle-shaped and occupied a significant surface area (Figure 5.5).

Based on the SEM observations, two distinct morphologies (nodular and flake) were present in the Zn-Ni coatings. A detailed EDS study was conducted to determine possible compositional differences in those two morphologies and also possible differences in each morphology as a function of the Ni content of the coatings. Thus, spot and small area analyses were conducted on these individual features. Figures 5.8, 5.9 and 5.10 present typical EDS spectra from these features for coatings 1C, 1D and 1E, respectively.

It can be observed that when the Ni content in the coatings is increased, such value is also increased in the nodular and flake phases as well. These observations suggest that these phases can exist with a variation in the Ni content. These results indicate that more flake phase is visible on the surface for coatings with higher Ni content. Table 5.2 summarizes these results.

Table 5.2 Morphology and average composition of coatings as determined by SEM/EDS.

Coating	**Composition***		**Morphology/Characteristics**	
	Zn at.%	Ni at.%	Nodules	Flakes
1A	82-84	16-18	Mostly coarse nodules (size 1-10 μm)	Very few observed
1B	~82	~18	Mostly finer nodules (1-5 μm)	Very few observed
1C	~75	~25	Nodules (~21% Ni) Nodule size ~4-10 μm	Flakes (~25% Ni) Flake size ~8-16μm
1D	78-80	20-22	Nodules (18.5-20% Ni) Nodule size 2-8 μm	Flakes (~22.5% Ni)
1E	68-70	30-32	Nodules (28-30% Ni) Nodule size 1-10 μm	Flakes (~33% Ni) Flake size ~1-2 μm

* Only Zn and Ni were considered.

The fact that more flakes are visible in coatings 1C, 1D and 1E, than coatings 1A and 1B can be explained by studying the chemical composition of each phase on its own. In coatings with a Ni content less than 20 wt.%, such element is found in more quantity in the nodular phase than

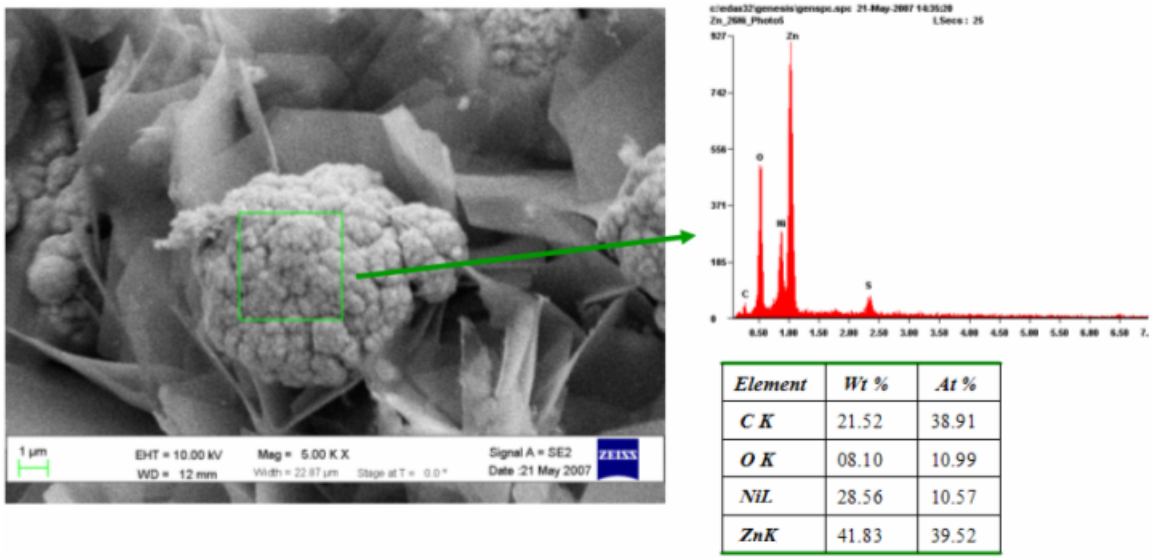

Element	Wt %	At %
C K	21.52	38.91
O K	08.10	10.99
NiL	28.56	10.57
ZnK	41.83	39.52

(a)

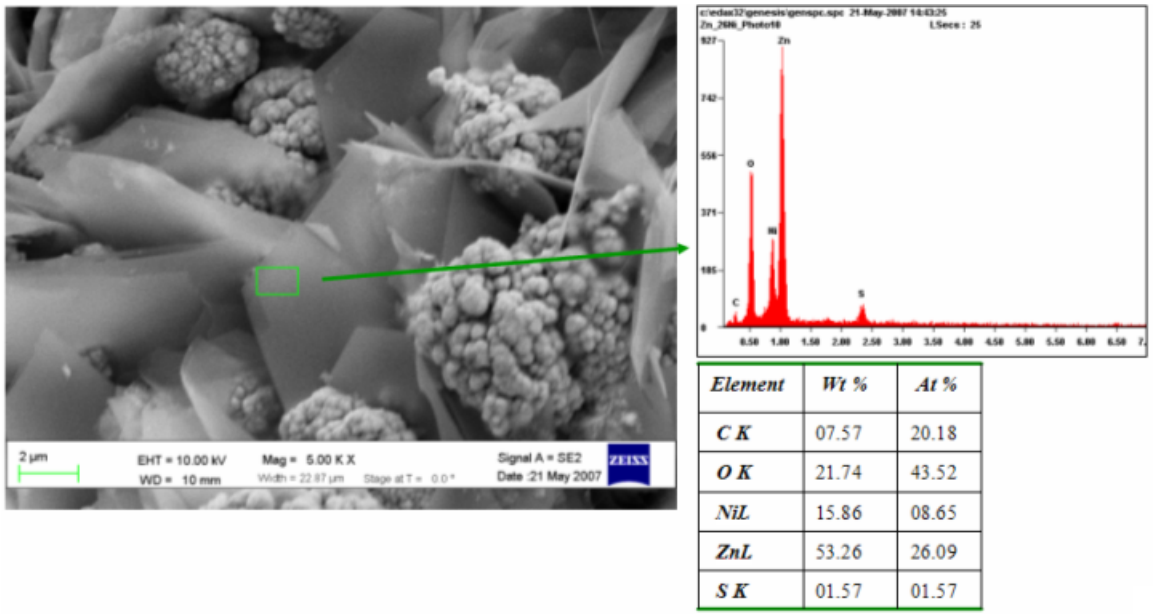

Element	Wt %	At %
C K	07.57	20.18
O K	21.74	43.52
NiL	15.86	08.65
ZnL	53.26	26.09
S K	01.57	01.57

(b)

Figure 5.8 Typical EDS spectra from the area shown in the micrograph for coating 1C: (a) nodular and (b) flake phase.

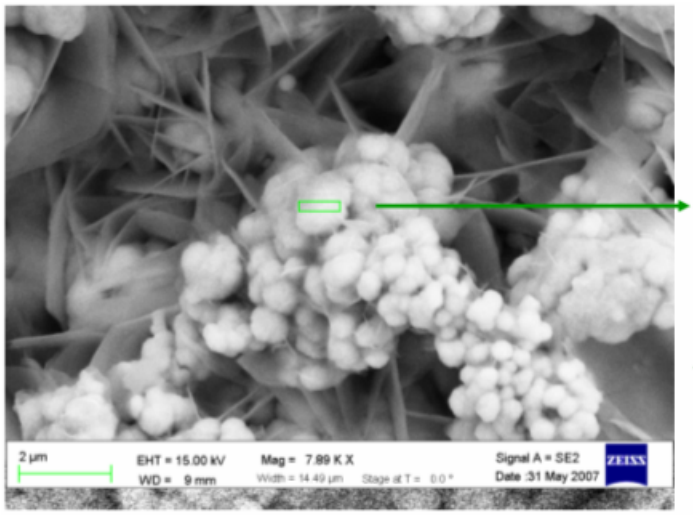

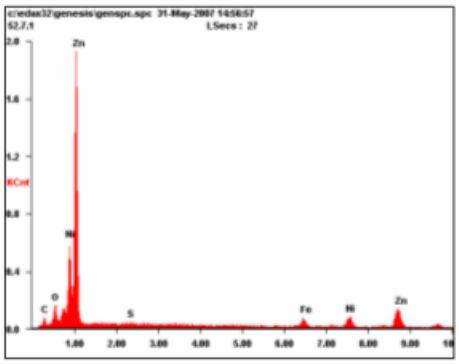

Element	Wt %	At %
C K	09.66	32.30
O K	05.44	13.65
S K	00.30	00.38
FeK	06.21	04.46
NiK	14.92	10.21
ZnK	63.48	39.00

(a)

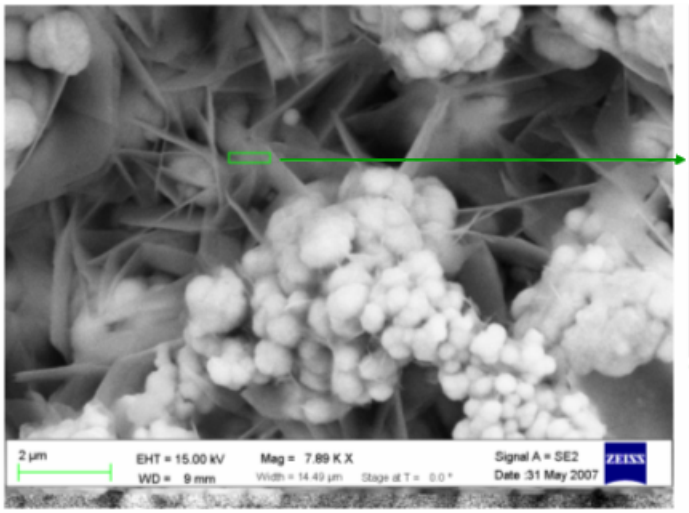

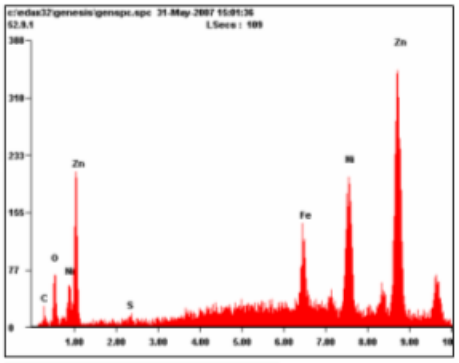

Element	Wt %	At %
C K	01.18	05.78
O K	00.95	03.49
S K	00.10	00.18
FeK	06.38	06.69
NiK	18.77	18.74
ZnK	72.62	65.12

(b)

Figure 5.9 Typical EDS spectra from the area shown in the micrograph for coating 1D: (a) nodular and (b) flake phase.

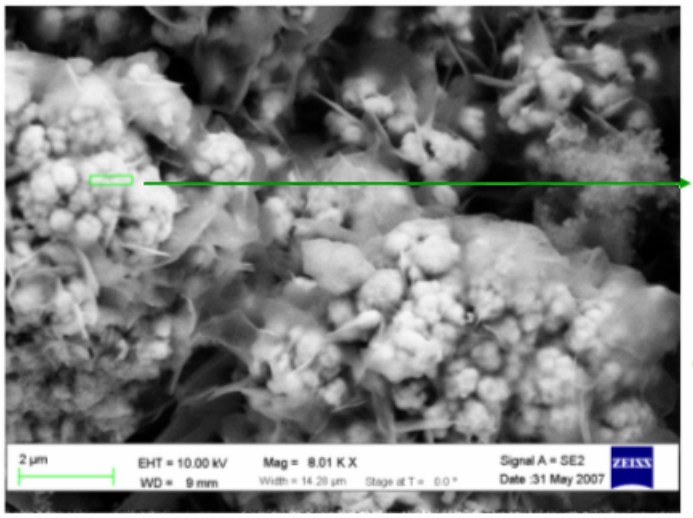

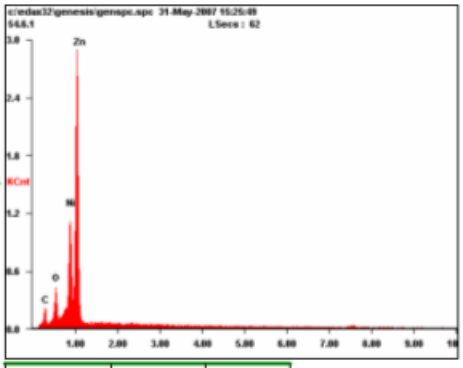

Element	Wt %	At %
C K	12.62	38.47
O K	06.52	14.92
NiL	20.81	12.98
ZnL	60.04	33.63

(a)

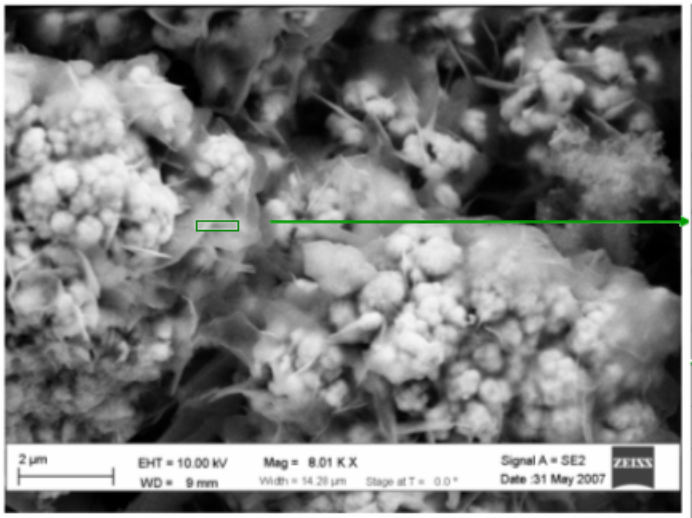

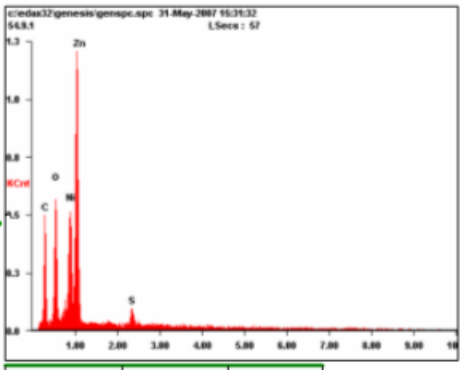

Element	Wt %	At %
C K	26.08	54.73
O K	12.71	20.03
NiL	18.80	08.07
ZnL	40.36	15.56
S K	02.04	01.61

(b)

Figure 5.10 Typical EDS spot spectra from the area shown in the micrograph for coating 1E: (a) nodular and (b) flake phase.

in the flake phase. This seems to suggest that when the nodular phase is present, Ni prefers to go into this phase rather than nucleating the flake phase. When the Ni content is increased above such value, it tends to go preferentially into the flake phase. This indicates that, even though both phases can dissolve Ni, the flake phase is capable of dissolving more Ni than the nodular phase [35].

Observations of cross sections by SEM showed that in general, the coatings were following the substrate surface profile (conformal) and occasionally exhibited some porosity and discontinuities, Figure 5.1(c). It should be pointed out that plasma discharge with bubble collapsing and shock wave production takes place also during coating (See section 3.2.3). This process occurs in both “hills” and “valleys” of the cleaned substrate resulting in deposition that follows the surface profile of the substrate. Such process is critical in providing mechanical interlocking for the coating improving adhesion.

It is also observed that occasionally coating deposition occurs preferentially on those places which can provide a shorter path to the discharge of the plasma. A typical example is shown in Figure 5.2(c) for coatings 1B. Another observation was that high Ni coatings appeared more dispersed, Figures 5.3(c), 5.4(c) and 5.5(c). This morphology is attributed to higher content of flake phase.

5.1.2 Structure analysis

The structural variation of Zn-Ni coatings as a function of the Ni content was investigated by XRD to provide an understanding of the grain morphology exhibited by the coatings (work conducted by Dr. S. You). The equilibrium phase diagram of the binary Zn-Ni system was used to provide background information about the observed morphologies, Figure 5.11. Also, Figures 5.12 -5.16 present the XRD patterns for Series 1 coatings.

The XRD results for coatings 1A and 1B, Figures 5.12 and 5.13, show that for both cases, Ni is mostly present in the γ phase. The phase diagram shows that the equilibrium phase can accommodate ~15 -27 at% Ni. It has been reported [3] that there may be two variations of this phase, one with low Ni content, γ_1 (Ni_5Zn_{21}), cubic structure with a major (3,3,0) reflection at

$2\theta = 42.88^{o}$, and one with high Ni content, γ_2 ($NiZn_3$), orthorhombic structure with two major reflections at $2\theta = 43.42^{o}$ from (8,1,5) and (16,0,0) planes. The Ni content determined for coatings 1A and 1B is consistent with the formation of the γ_1 phase which exhibits a nodular morphology. Another possible phase from the equilibrium phase diagram is stoichiometric δ Ni_3Zn_{22}, however its formation has not been reported yet under plating conditions.

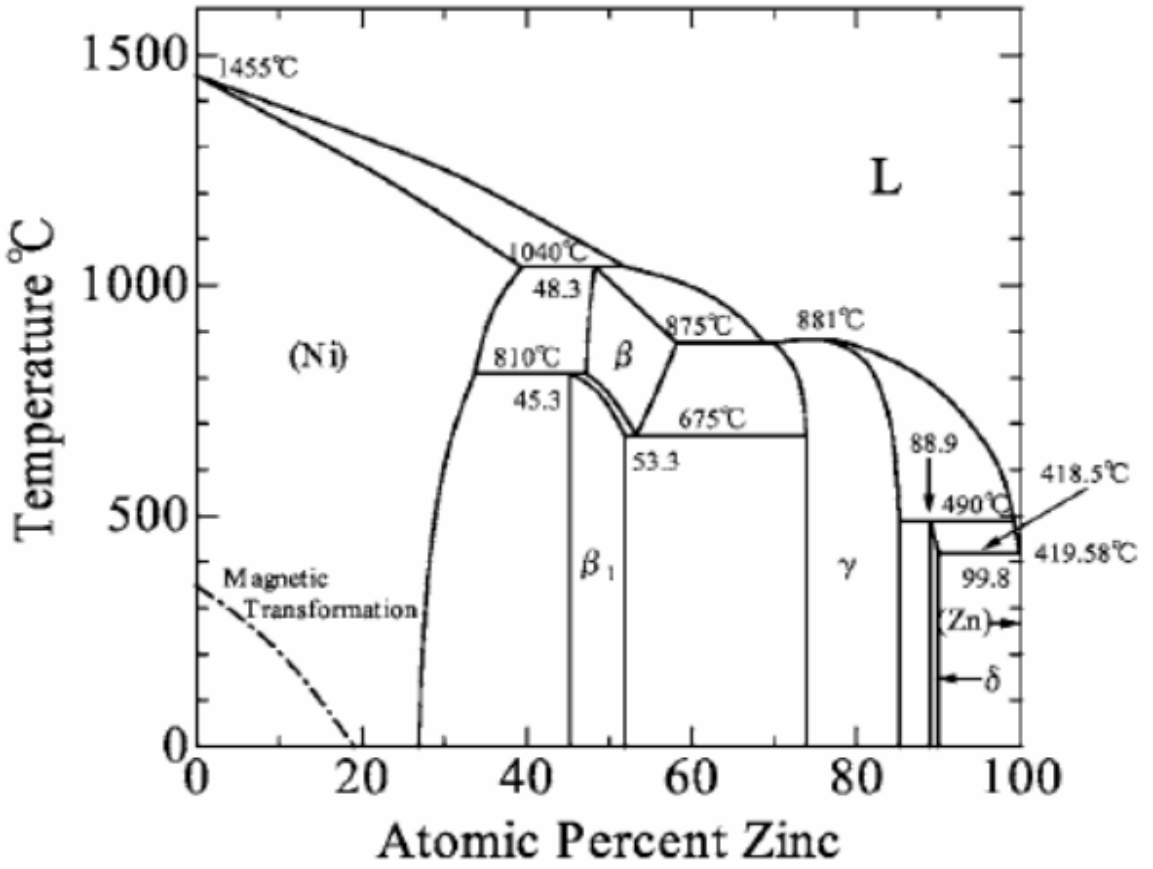

Figure 5.11 Ni-Zn equilibrium binary phase diagram [34].

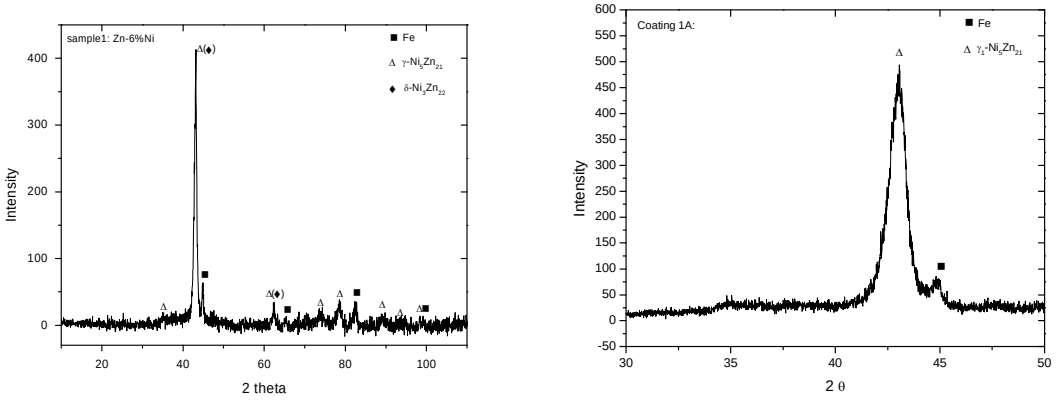

(a) (b)

Figure 5.12 XRD pattern of coating 1A.

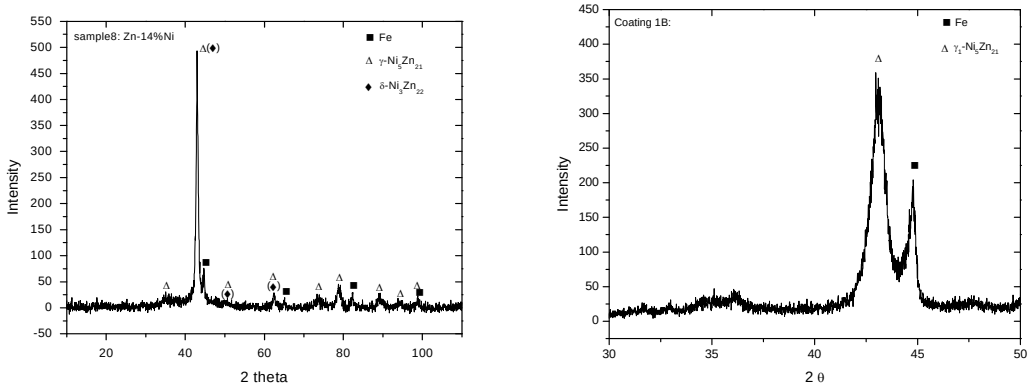

(a) (b)

Figure 5.13 XRD pattern of coating 1B.

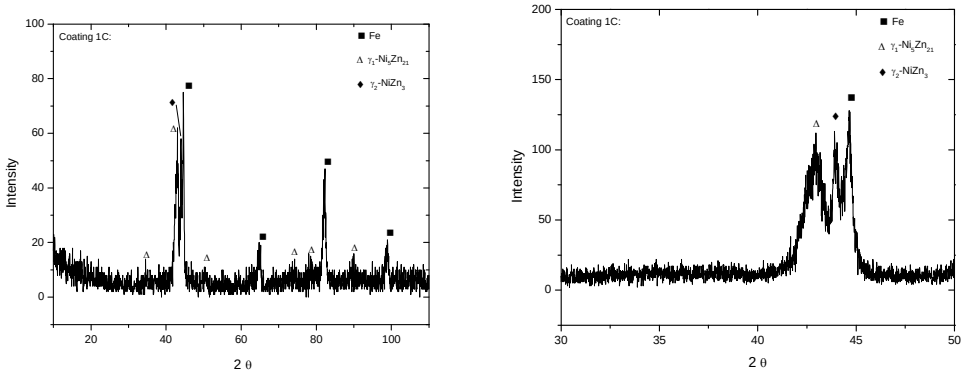

(a) (b)

Figure 5.14 XRD pattern of coating 1C.

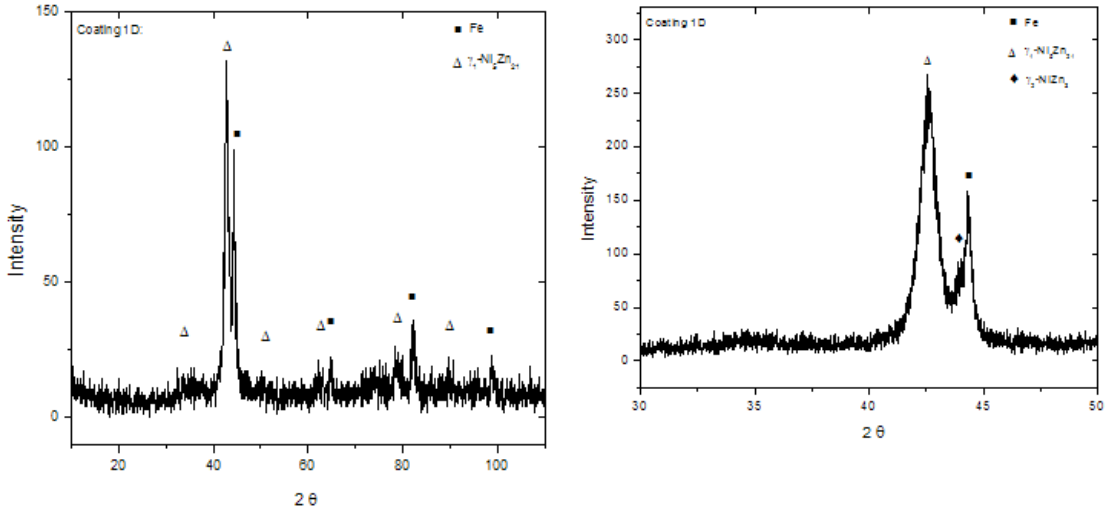

(a) (b)

Figure 5.15 XRD pattern of coating 1D.

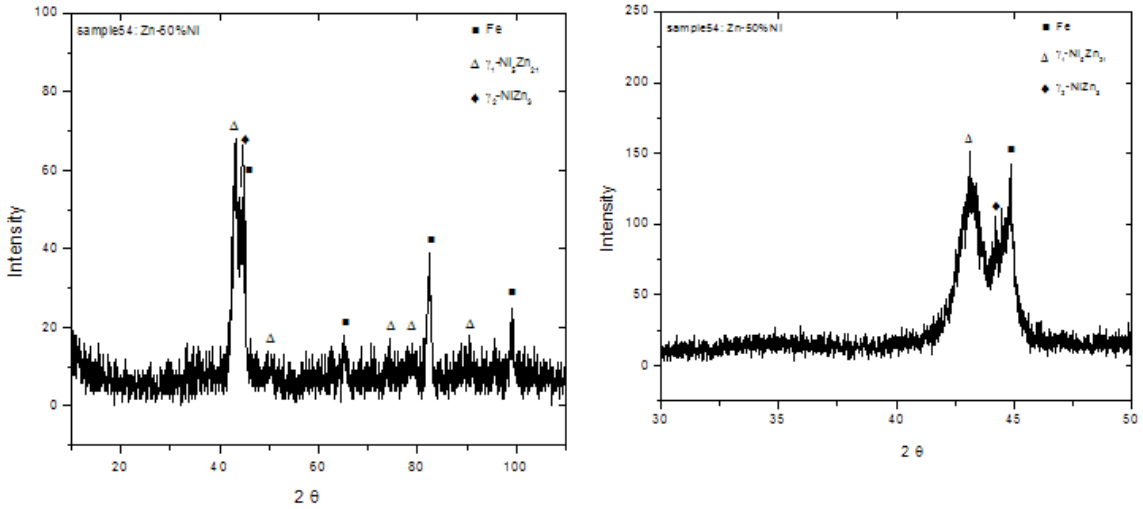

(a) (b)

Figure 5.16 XRD pattern of coating 1E.

XRD analysis of coating 1C, 1D and 1E, Figure 5.14, 5.15 and 5.16, respectively, in general, shows evidence of phases γ_1 and an additional phase with a major peak at $2\theta = 43.42°$. The present microstructural observations suggest that this phase corresponds to the flake phase. This phase was present in coatings 1C, 1D and 1E that showed presence of this diffraction peak at 43.42^o. Further more, this phase has been identified previously as γ_2 phase [36,37,38].

In view of the high O content of the Zn-Ni coatings (Table 5.1) and the morphology of the flake phase that this is an oxide phase. There are two dominant structures for NiO: a cubic structure with major peaks at $2\theta = 37.092°$, 43.095°, and 62.584° corresponding to (111), (200), and (220) planes, respectively, and a rhombohedral structure with major peaks at $2\theta = 37.248°$, 43.286°, 62.852° from (101), (012), and (110) planes, respectively. Neither of these structures is consistent with the present XRD. Further more, it should noted that coatings 1D and 1E contained less O than coating 1C however, showed significant presence of the flake phase. Finally, EDS analysis from flakes in coating 1D, Figure 5.9(b), showed very low O content for this phase to correspond to an oxide. Thus, more than likely, the flake phase corresponds to γ_2 that grows preferentially along the orthorhombic [8,1,5] and [16,0,0] directions resulting in a plate like shape.

It is interesting to note that coating 1E exhibited very broad peaks at the 2θ positions corresponding to γ_1 and γ_2 phases. This is attributed to the fine size of these two phases as observed by SEM. EDS analysis showed that both the nodules (corresponding to γ_1) and flakes (corresponding to γ_2) accommodate more Ni (~28 at%Ni for nodules, γ_1 and ~33 at%Ni for flakes, γ_2) than in the previous coatings. These limits are beyond the equilibrium limits however, they are possible since deposition takes place under non equilibrium conditions.

5.1.3 Electrochemical characterization

Figure 5.17 shows the variation of E_{corr} with time for Series 1 coatings in tap water. Under general corrosion considerations, for a metallic coating to electrochemically protect a steel substrate, its potential should be more active than that of steel. This means that the electrochemical potential of the steel should have a greater value than those of the coatings [35,36]. That is, all coatings but 1A, will not be in a position to provide electrochemical protection

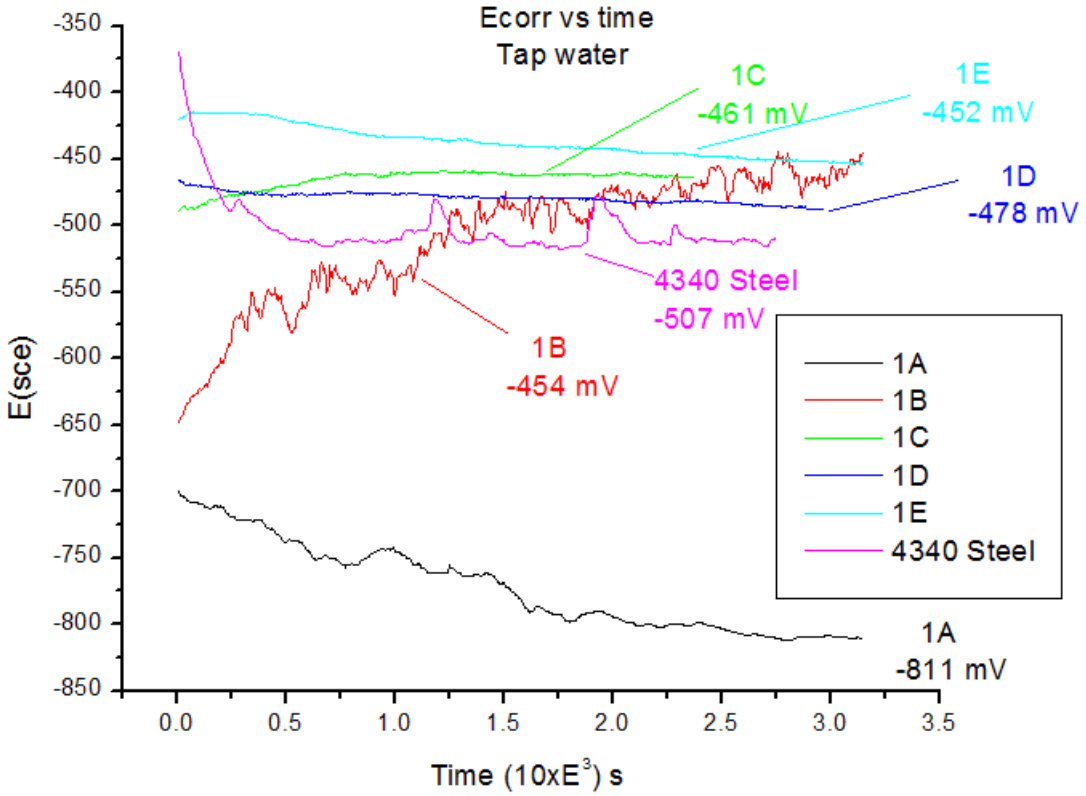

Figure 5.17 Variation of the corrosion potential as a function of immersion time for Series 1 coating in tap water.

to the substrate. Figure 5.17 clearly shows a trend between Ni content and E_{corr}. Incorporation of Ni that has a noble potential drives the coating potential to higher values. The results show that all high Ni content coatings (1C, 1D and 1E) exhibited a more noble potential than that of steel. Only coating 1A exhibited a potential lower than that of steel. Thus, this is the only coating that can act as a sacrificial anode providing corrosion protection.

It is interesting to note that coating 1B shows a transient behavior. The E_{corr} is low initially but raises with time reaching the corrosion potential of steel in about 1250 s and subsequently surpassing it. This behavior can be attributed to galvanic corrosion at the atomic scale. Initially Zn atom dissolution occurs preferentially from the γ_1 phase. This is very similar to dezincification that takes place in brass (Cu-Zn alloy) and other alloys composed of elements with large differences in their electrochemical potential. As the coating is depleted from Zn, a Ni-rich layer remains and the potential moves in the noble direction. This behavior of the coating can also be interpreted by considering the results of the morphological and structural studies. All coatings with significant presence of the high-Ni γ_2 phase (1C, 1D and 1E) exhibited higher corrosion potentials. Coatings composed of the low-Ni γ_1 phase (1A and 1B) exhibited low corrosion potentials. Thus, coating behavior can be associated not just to Ni content but more significantly to the presence of γ_1 and γ_2 phases.

Figure 5.18 presents the anodic polarization behavior of Series 1 coatings in tap water. The results are consistent with the E_{corr} measurements. The kinetic information shows that all coatings but 1A show higher potential than steel. Furthermore, it is interesting to note that the corrosion rate of the coatings increases as the Zn content is increased. Higher corrosion rates were observed in the more aggressive NaCl environment compared to tap water. The corrosion rates exhibited by all present Zn-Ni coatings were found to be higher than that of steel. This result may indicate that, as it was reported on the literature [43], by increasing the Ni content is possible to reduce the electrochemical kinetics of Zn-Ni coatings. Table 5.2 could explain in part the anodic polarization behavior described above. That is, when Ni content of the system is increased, two electrochemically different phases co-exist, the noble Ni-rich γ_2 phase and the

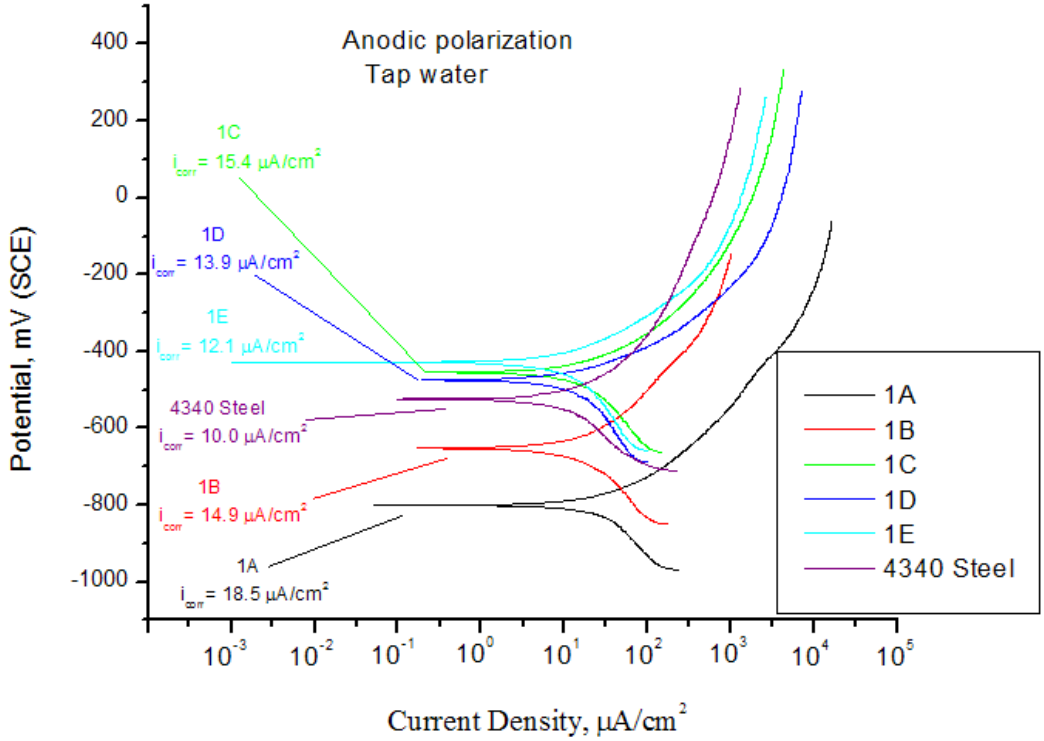

Figure 5.18 Anodic polarization behavior of Series 1 coatings in tap water.

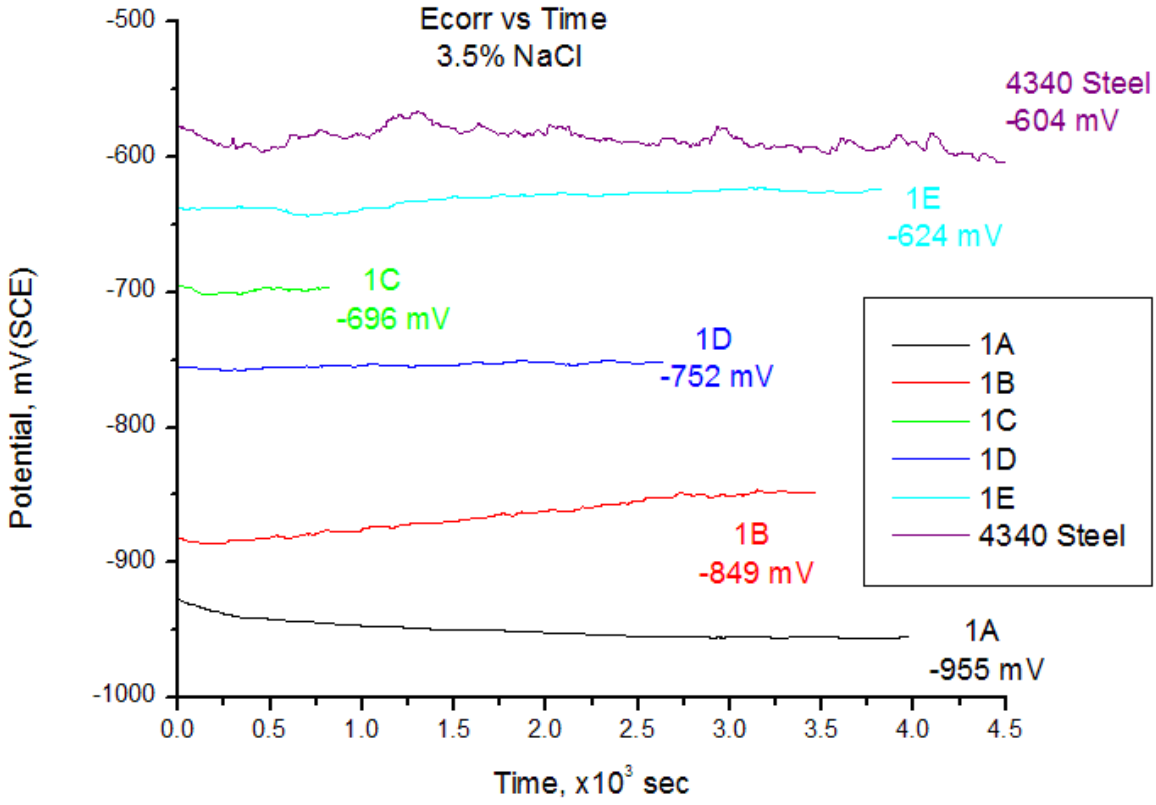

Figure 5.19 Variation of the corrosion potential as a function of immersion time for Series 1 coatings in 3.5% NaCl solution.

active Zn-rich γ_1 phase. This effect promotes the formation of galvanic couples with a driving force for Zn dissolution [40,41,42]. Yet, since Ni is fairly distributed in both phases that driving force between the anodic and cathodic regions is not very significant as shown by the low corrosion rates of the Ni-rich coatings [43,44]. On the contrary, a more significant effect is observed from atomic galvanic cells that exist in coatings 1A and 1B where only one phase (γ_1) is present. This is evident from the high corrosion rates shown by the latter coatings.

Figure 5.19 shows the variation of E_{corr} vs. time for the Series 1 coatings in 3.5% NaCl solution. As it was expected, the potential values are lower when compare with those obtained from tap water since the electrolyte used is electrochemically more aggressive. It is notablethe E_{corr} variation follows a similar pattern which was observed in Figure 5.17. That is coatings 1C, 1D and 1E, which had higher Ni content as well as γ_2 phase (flake phase) have higher E_{corr} or less active potentials than low Ni content coatings 1A and 1B. This clearly confirms that those coatings with higher Ni content will have more noble potentials than those with lower Ni content also in the NaCl environment.

Steel in 3.5% NaCl solution exhibited a potential of -604 mV, which is more noble than all of the coatings. This indicates that under 3.5% NaCl such coatings from Series 1 will electrochemically protect the underlying steel structure. However, these results show that in a more drastic environment such as NaCl, the corrosion behavior may be reversed from that in tap water. The electrochemical kinetics may change in a more aggressive environment resulting in a variation of the corrosion behavior.

Figure 5.20 shows the anodic polarization behavior of Series 1 coatings tested in 3.5% NaCl solution. As it was stated previously, a NaCl is electrochemically more aggressive than tap water, thus not only E_{corr} values will be more active but corrosion rate values are greater. Also, coatings with higher Ni content tend to dissolve slower than those with lower Ni content. That is, coating 1A exhibits a i_{corr} of 61.7 $\mu A/cm^2$ meanwhile 1E exhibits a i_{corr} of 30 $\mu A/cm^2$. This behavior indicates that Ni content by itself and the morphologies formed on the surface associated with it, are responsible for the observed corrosion behavior of the coatings.

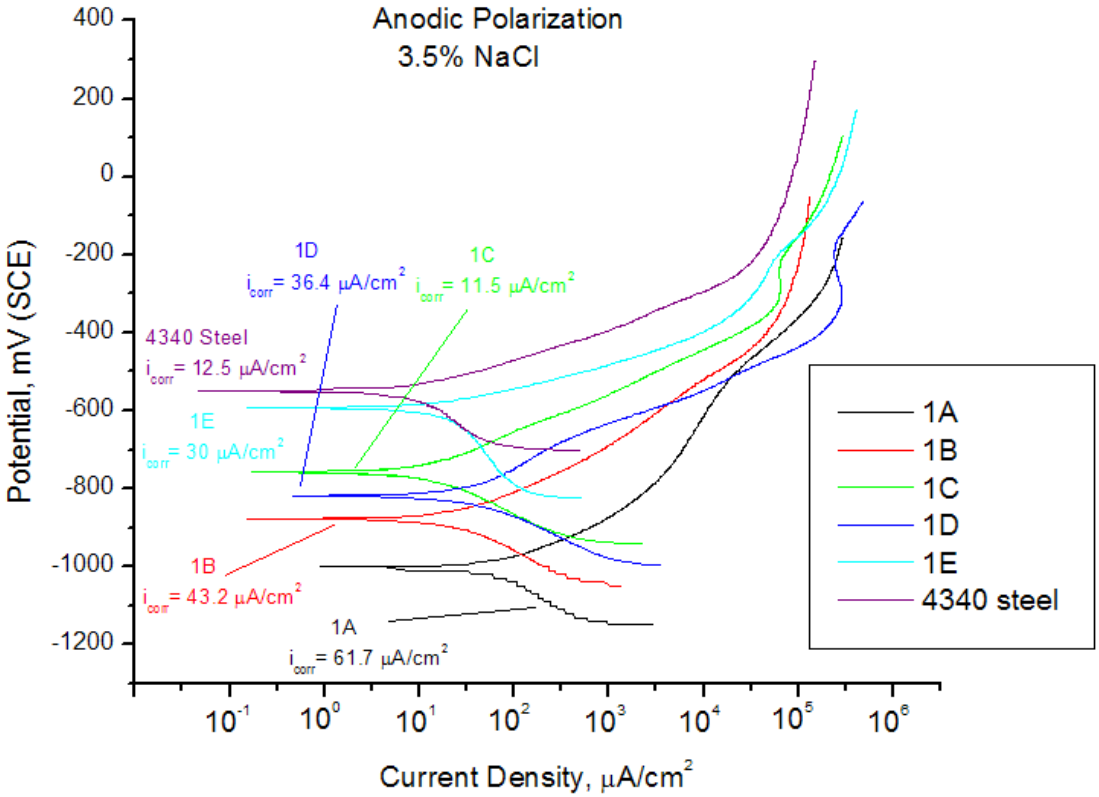

Figure 5.20 Anodic polarization behavior of Series 1 coatings in 3.5 % NaCl solution.

Table 5.3 summarizes the corrosion potential and corrosion rate exhibited by all Series 1 coatings. Values for steel are also shown for comparison purposes.

After characterizing Series 1 coatings, it can be concluded that the chemical composition, surface morphology, structure and electrochemical properties of Series 1 coatings, are related to the Ni content and those morphologies associated with it. Coatings with low Ni content are composed of nodular-type phse exhibiting lower E_{corr} and higher corrosion rates. Those coatings with higher Ni content have significant presence of flake phase, higher E_{corr} and lower corrosion rates. It was also observed that since increasing the Ni content also increases the potential, after such element reaches a compositional threshold, the coating ceases to act as sacrificial anode. Such value is around 20 wt.% Ni [43,45,46,47].

Table 5.3 Corrosion potential and corrosion rate for Series 1 coatings in tap water and 3.5% NaCl solution under laboratory air conditions.

Property	E_{corr}, mV		i_{corr}, μA/cm^2	
Coating	Tap Water	3.5% NaCl	Tap Water	3.5% NaCl
1A	-811	-955	18.50	61.70
1B	-454	-850	14.90	43.20
1C	-461	-700	15.40	11.50
1D	-478	-752	13.90	36.40
1E	-452	-624	12.10	30.00
Steel	-506	-604	10.00	12.50

5.1.4 Surface morphology and chemical characterization after electrochemical testing

After undergoing electrochemical testing (corrosion potential and anodic polarization behavior) in 3.5% NaCl solution under laboratory conditions, the surface morphology of coating 1E was studied with SEM. Originally, it was observed that coating 1E had a significant presence of flake phase or γ_2 as well as γ_1 or nodular phase, Figure 5.5 and Table 5.2. After corrosion testing, it was observed that the presence of the nodular phase on the surface was severely

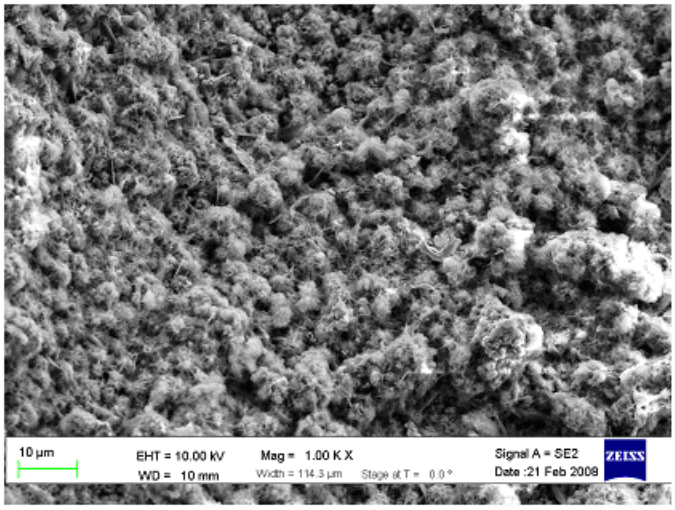

(a)

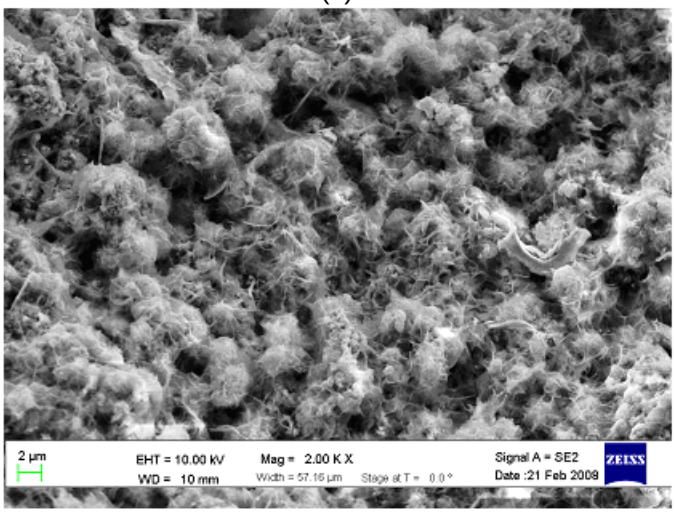

(b)

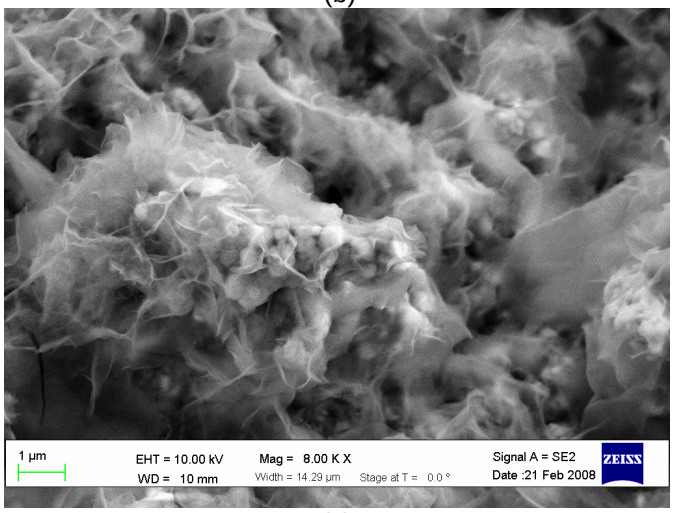

(c)

Figure 5.21 SEM micrographs of coating 1E: (a) overall surface morphology, (b) and (c) high magnification of (a).

reduced, Figure 5.21, generating a surface composed principally of the flake phase. As discussed earlier, this observation clearly shows that the Zn-rich phase was more active and thus, underwent anodic dissolution. The more noble Ni-rich γ_2 phase being cathodic with respect to the γ_1 phase remained in place. This result indicates that the Zn-rich phase will corrode and dissolve preferentially. Such phenomena were expected since Ni has a less active corrosion potential compared to Zn. So, the nodular phase will act as anodic region whereas the flake phase will act as cathodic region. This electrochemical couple results in the subsequent dissolution of Zn atoms present in γ_1 [48,49]. In order to gain more insight in the above process, the chemical composition was obtained prior to and after electrochemical testing from the surface of coatings 1E, Table 5.4. Oxygen, as it was expected, has increased more than 20 wt.% as a direct result of the corrosion products attached to the surface which were generated during the electrochemical process. The Zn content was reduced by almost 10 wt.% whereas the Ni content showed an increase. Alternatively, comparing the Zn/Ni ratio, the results show a more than 40% reduction of this ratio. This indicates that, in accordance with Figure 5.21, Zn-rich phases are corroding preferentially than the Ni-rich ones. Finally Fe has also increased by ~3%. This indicates that the coating thickness has decreased due to the corrosion process and there were contributions from the steel substrate to the compositional analysis.

Table 5.4 Elemental composition by EDS analysis from the surface of coating 1E taken prior to and after corrosion testing in 3.5% NaCl solution.

Element wt.%	Ni	Zn	Fe	O
As-deposited	11.67	25.09	1.08	17.25
After testing	13.66	16.51	4.13	38.67

After characterizing Series 1 coatings, it can be concluded that the chemical composition, surface morphology, phases present, structure and electrochemical properties are directly related to the Ni content and those morphologies and phases associated with it. Coatings with low Ni content are mainly composed of nodular-type Zn-rich phase exhibiting lower E_{corr} and higher i_{corr}

Values. Coatings with higher Ni content have a significant presence of the flake-type Ni-rich phase, higher E_{corr} and lower i_{corr} values. It was also observed that since increasing the Ni content also increases the potential, after this element reaches a compositional threshold, the coating will cease to act as a sacrificial anode providing corrosion protection. Such value is around 18 wt.% Ni. This is in agreement with previous reports in the literature from electrodeposited Zn-Ni coatings [40,44,45,46].

5.2 Characterization of Series 2 coatings

5.2.1 Morphology and composition

Based on the results of Series 1 coatings, this part of the study concentrated on lower Ni content coatings and on the effect of conversion coatings (Dipsol and Metalast). Figure 5.22 presents typical surface morphologies of Series 2 coatings. All are primarily made of γ_1 phase (nodules). Coatings 2B and 2C show also, at greater or lesser degree, presence of γ_2 phase (flakes). Figures 5.22(a) and 5.22(d) show the surface morphology of coatings 2A and 2D that were treated by Dipsol. No flakes are visible.

Table 5.5 summarizes the chemical composition of the 4 coatings from Series 2. It is evident that the present coatings have lower Ni content compared to Series 1. Also, conversion coatings have been applied to coatings 2A, 2D (Dipsol) and 2B (Metalast). When the surfaces of Series 2 coatings are compared with Series 1 coatings with similar Ni content, similar morphologies are expected to be present on the surface. Yet, coatings 2A and 2D discern somewhat different surface morphologies when compared to coatings 1B and 1D. SEM observations indicate that Dipsol is preferentially interacting with the flake phase. On the other hand, coating 2B which was treated with Metalast, Figure 5.22(b), discerned an abundant of the flake phase on the surface. This indicates that Metalast conversion coating was interacting with the nodular phase.

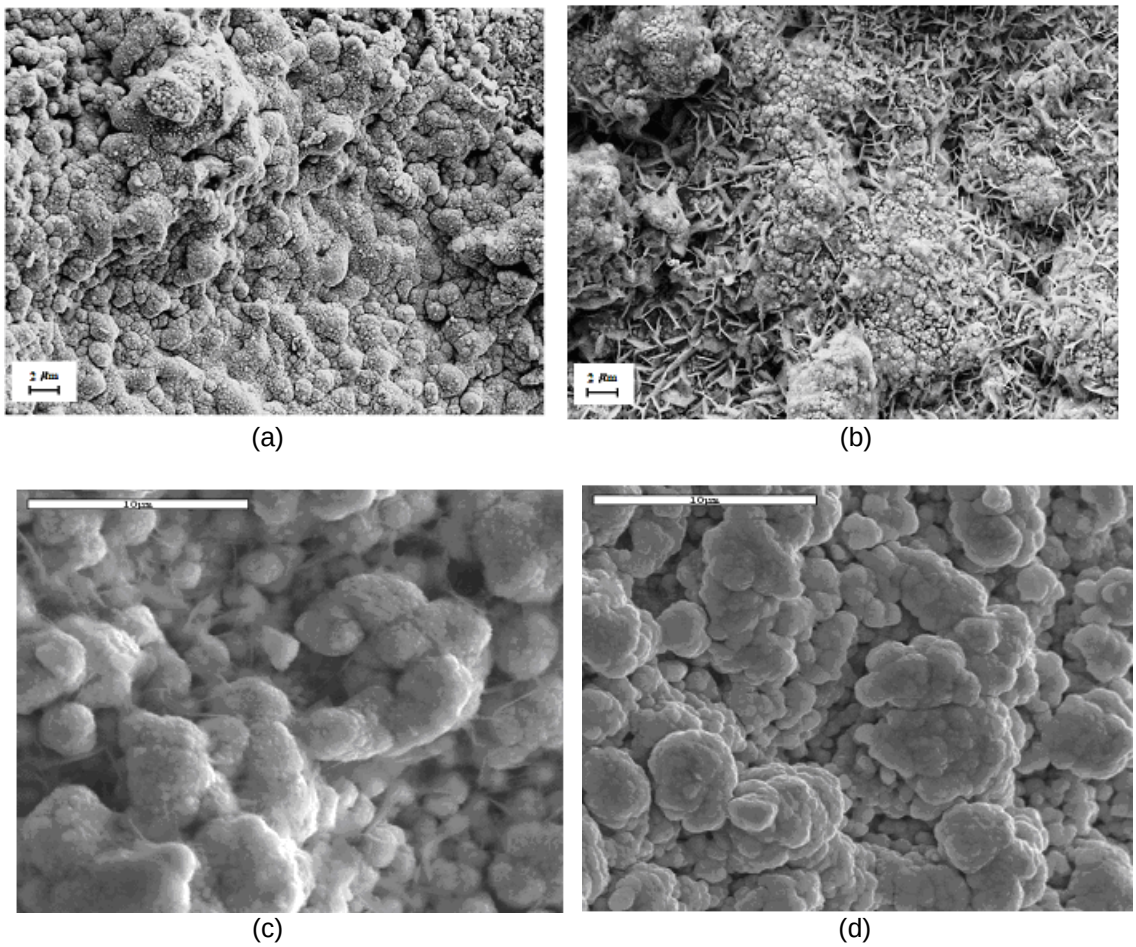

Figure 5.22 SEM micrographs of Series 2 coatings: (a) 2A, (b) 2B, (c) 2C and (d) 2D.

Table 5.5 Chemical composition of Series 2 Zn-Ni coatings obtained by EDS.

Coating	Conversion Coating	Ni		Zn		O		Fe		*Ni/Zn	
		wt%	at %	wt%	at %	wt%	at %	wt%	at %	wt.%	at.%
2A	**Dipsol	16.62	14.57	71.40	56.21	7.92	25.49	4.05	3.74	18.5/81.5	20.2/79.8
2B	***Metalast	15.79	11.63	65.99	43.66	15.86	42.88	2.36	1.83	19.1/81.0	20.8/79.2
2C	NA	18.01	14.25	66.42	47.19	12.36	35.89	3.21	2.67	21.0/79.0	22.8/77.2
2D	Dipsol	19.67	13.42	54.72	33.52	19.43	48.63	6.19	4.44	25.9/74.1	28.0/72.0

* Composition based only on Zn and Ni
** IZ 258 (Hexavalent chromate based)
** TCP-HF (Trivalent chromate based)
NA: Not Applied

5.2.2 Electrochemical characterization

The variation of the corrosion potential with time and the anodic polarization behavior in tap water and 3.5% NaCl solution for all Series 2 coatings and 4340 steel are shown in Figures 5.23, 5.24 and 5.25. The stabilized corrosion potential values along with the corrosion rates for all coatings are summarized in Table 5.6.

The corrosion potential results, Figure 5.23, show that all specimens exhibit an anodic potential with respect to that of 4340 steel (-533 mV) in tap water except 2D (-504 mV) which was more noble than steel. This particular specimen was treated by Dipsol but had the highest Ni content reaffirming the previous observations that high Ni content promotes nobility and does not qualify as a sacrificial coating for steel. Also, coating 2C exhibited a corrosion potential (-536 mV) similar to that of steel and does not qualify either for such an application.

Table 5.6 Corrosion potential and corrosion rate for Series 2 coatings in tap water and 3.5% NaCl under laboratory air conditions.

Property	E_{corr}, mV		i_{corr}, μA/cm^2	
Coating	Tap Water	3.5% NaCl	Tap Water	3.5% NaCl
2A	-571	-811	3.43	3.76
2B	-587	-768	3.57	3.26
2C	-536	-713	4.40	3.86
2D	-504	-757	0.33	4.63
4340 Steel	-533	-728	12.60	78.90

In the NaCl environment, only coating 2C exhibited a higher potential (-713 mV) than that of steel (-728 mV) with coatings 2D being also close to that of steel in this environment. Based on these results, coatings 2C and 2D do not qualify as sacrificial coatings. Note that the latter two coatings had the highest Ni content among the Series 2 coatings. Thus, only the low Ni content coatings 2A and 2B treated with conversion coatings qualify as sacrificial anodes.

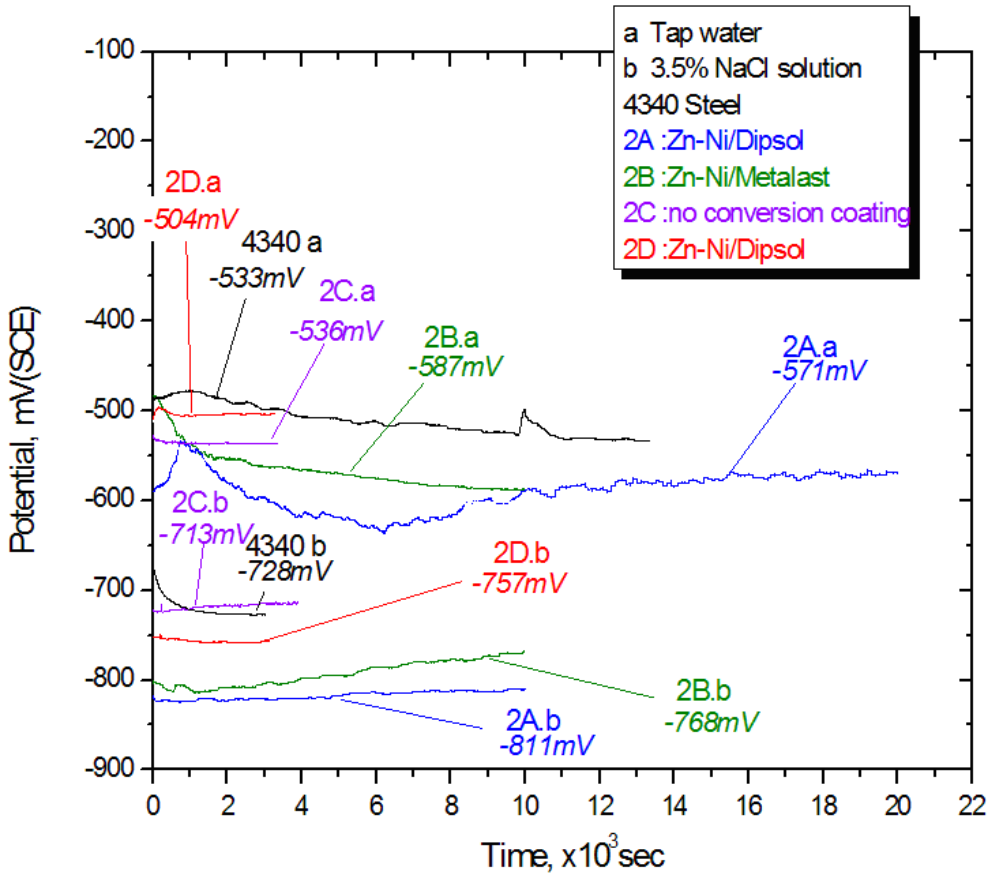

Figure 5.23 Variation of the corrosion potential as a function of immersion time for Series 2 coatings in tap water and 3.5% NaCl solution.

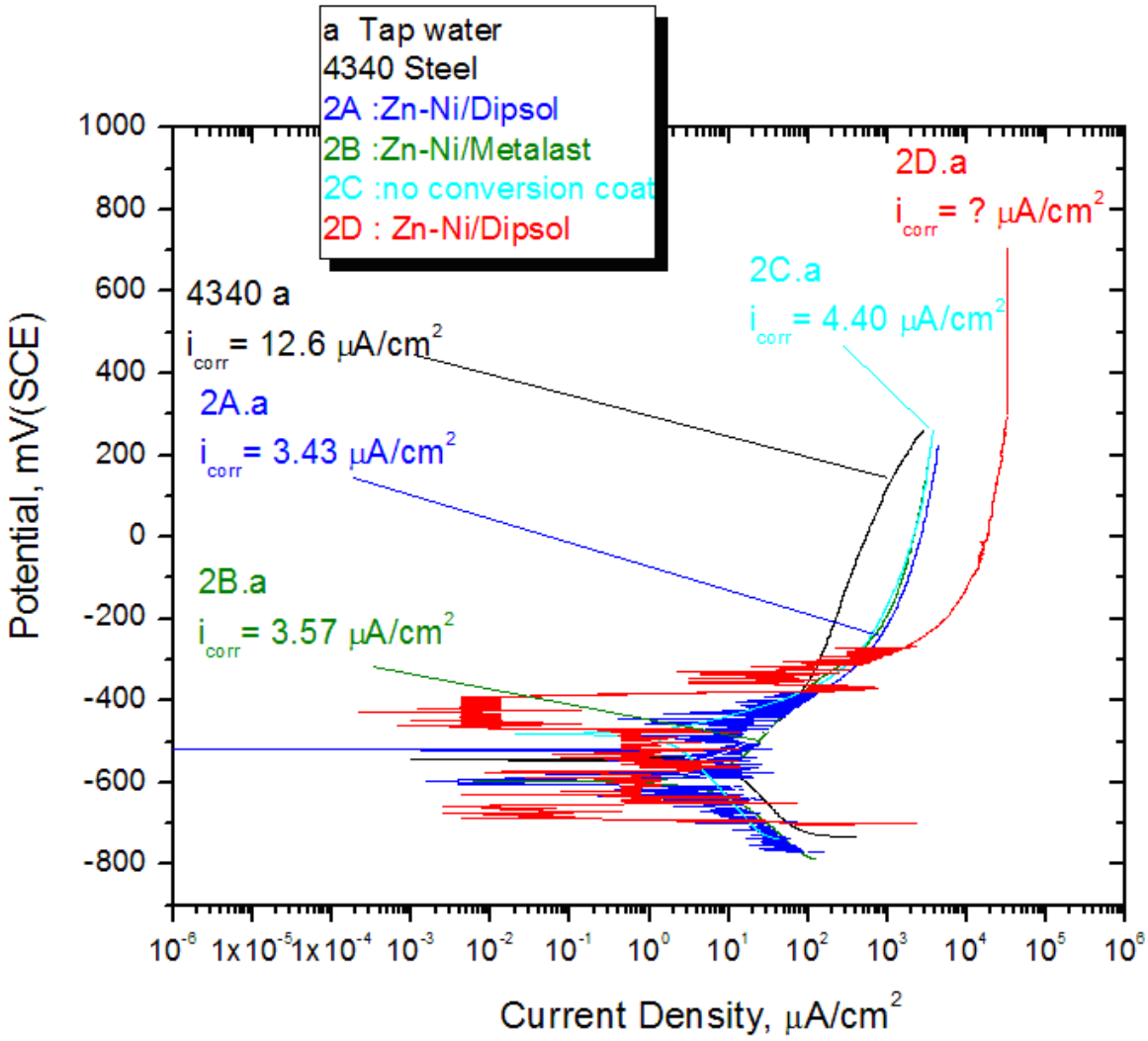

Figure 5.24 Anodic polarization behavior of Series 2 coatings in tap water.

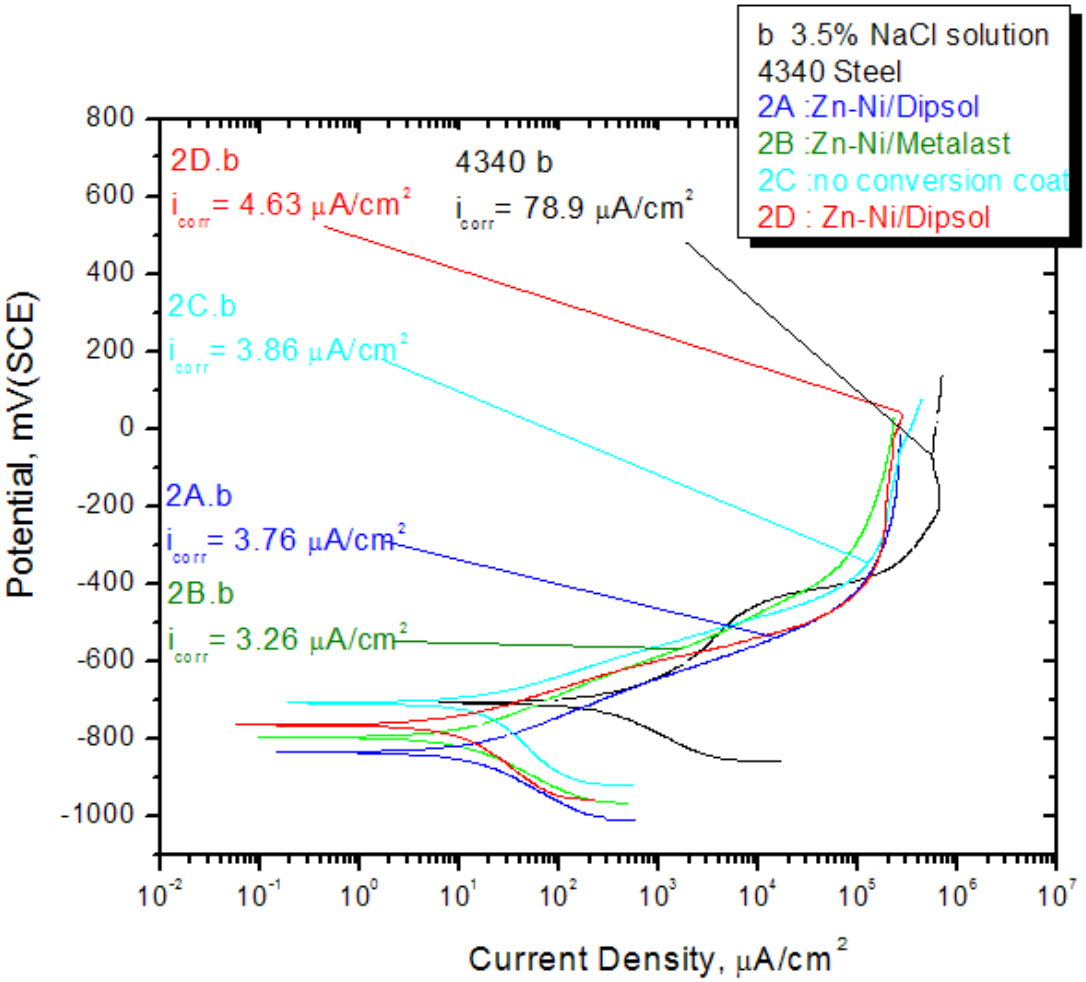

Figure 5.25 Anodic polarization behavior of Series 2 coatings in 3.5 % NaCl solution.

The effect of the conversion coatings on E_{corr} can be studied by comparing values for coatings 2B with 1C. Note that they both have a similar Ni content. In tap water, Coating 2B exhibited an E_{corr} = -587 mV whereas for coating 1C E_{corr} = -461 mV in the same electrolyte. The same effect seems to occur for coatings 2A and 2D in both electrolytes when compared with similar Ni content coatings from Series 1. This indicates that application of a conversion coating over the Zn-Ni coating results in a reduction of the E_{corr} or causes a significant activation of the surface. Thus, the E_{corr} measurements show that only the low Ni content coatings 2A and 2B are anodic with respect to steel. As mentioned earlier, both of these coatings were treated by conversion coatings and their E_{corr} values are lower than those of their counterparts from Series 1 without any conversion treatment. Thus, the conversion treatment offers the opportunity to further decrease the potential of these Zn-Ni coatings, if desirable.

Contrasting the anodic polarization behavior of Series 2 coatings 2A and 2B (~18-19 wt% Ni) with conversion treatment (Dipsol or Metalast) with coatings 2C of comparable Ni content (~21 wt% Ni) but without conversion treatment, an important observation can be made. It was observed earlier that application of the conversion coatings reduces the corrosion potential. Examining Table 5.6, it can be seen that even though coatings 2A and 2B have lower E_{corr} (smaller driving force), they also exhibit lower i_{corr} in both environments (tap water and NaCl solution) compared to coatings 2D. Thus, conversion coatings can change electrochemical kinetics resulting in a lower dissolution rate. This behavior may be particularly useful since the results show that low Ni content coatings with conversion treatment can be anodic to the steel structure with a significant difference in E_{corr} but at the same time will dissolve at a slower rate extending the lifespan of the Zn-Ni coating.

In summary, low Ni content coatings 2A and 2B treated with conversion coatings were found to be suitable as sacrificial anodes. Application of conversion coatings was found to provide additional advantages by lowering E_{corr} and i_{corr} at the same time.

5.3 Characterization of Series 3 coatings

5.3.1 Morphology and composition

A final set of low Ni content Zn-Ni coatings was prepared on flat panels intended for aggressive salt fog corrosion testing. This is an ASTM Standard test for sacrificial coatings. This test was conducted in an outside commercial testing facility. Prior to sending the coated panels for salt fog testing, all Zn-Ni coatings were characterized in terms of morphology, composition and corrosion behavior. In order to obtain a further understanding of the corrosion behavior, tests were conducted in both open laboratory air and deaerated conditions by purging Ar in the electrolyte.

Figure 5.26 presents typical surface morphologies of Series 3 coatings. Mainly a nodular phase was present similar to coatings in Series 1 and 2. The chemical composition and Zn-Ni ratio of all five coatings in Series 3 is presented in Table 5.7. Low Ni content was used and conversion coatings were applied to samples 3B (Dipsol) and 3C (Metalast).

5.3.2 Electrochemical characterization

The variation of the corrosion potential with time and the anodic polarization behavior of all five coatings for Series 3 and 4340 steel in tap water and 3.5% NaCl solution are shown in Figures 5.27, 5.28 and 5.29 for aerated (laboratory air) conditions and in Figures 5.30, 5.31 and 5.32 for deaerated conditions. The stabilized corrosion potentials and corrosion rates for all specimens for both conditions are listed in Table 5.8.

For laboratory air testing, the results showed that all coatings exhibited an active potential with repect to steel in tap water. However, in NaCl solution only coatings 3A and 3B exhibited a more active potential than steel, Figure 5.27. In fact, these were the coatings with the lowest Ni content, confirming the early findings. Similarly, for deaerated testing conditions, only coatings 3A and 3B were found to exhibit an active potential with respect to steel in both tap water and NaCl solution.

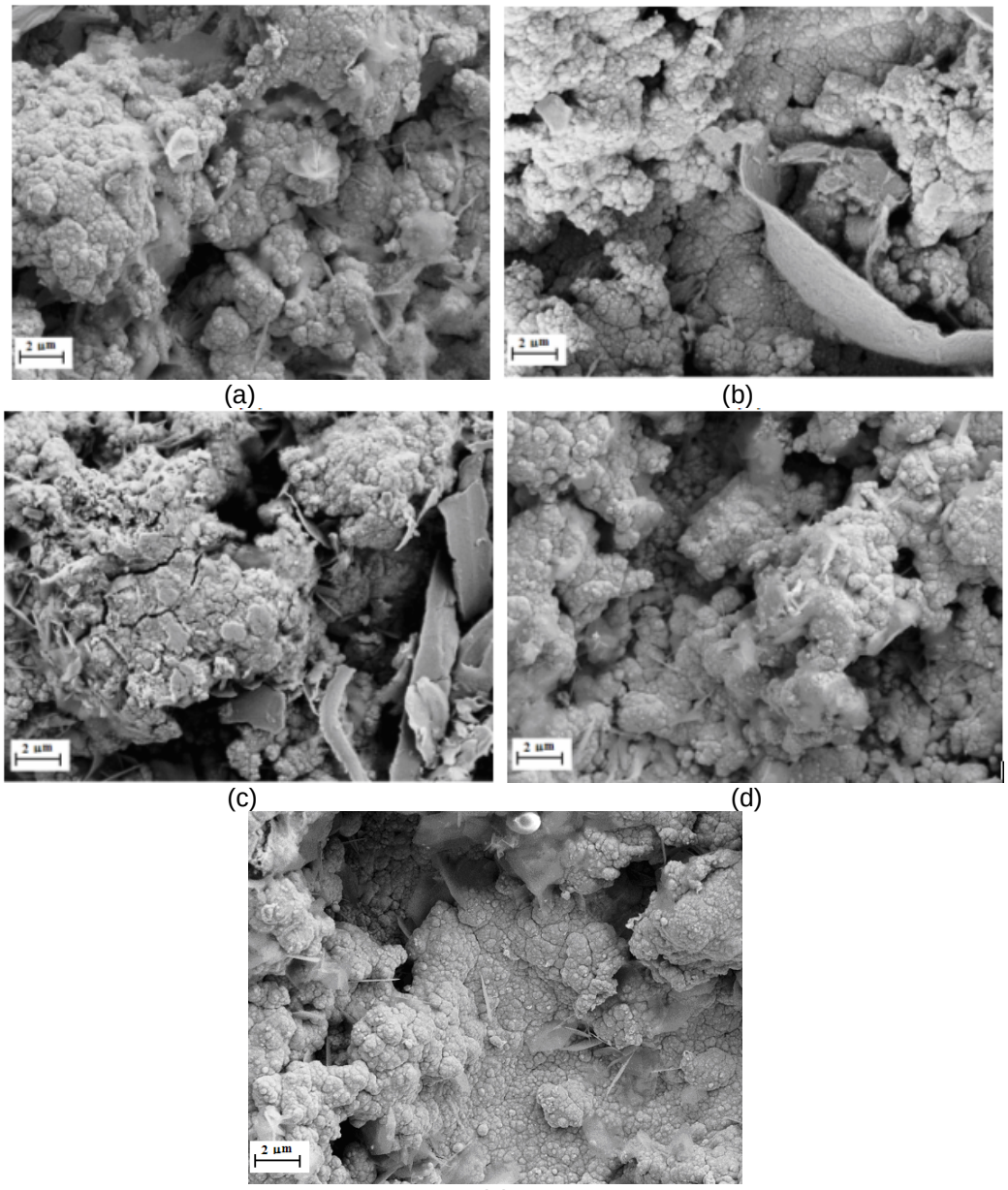

Figure 5.26 SEM micrographs of Series 3 coatings: (a) 3A, (b) 3B, (c) 3C, (d) 3D, and (e) 3E.

Table 5.7 Chemical composition of Series 3 Zn-Ni coatings obtained by EDS.

Coating	Conversion Coating	Ni		Zn		O		C		*Ni/Zn	
		wt.%	at.%	wt.%	at.%	wt.%	at.%	wt.%	at.%	wt.%	at.%
3A	NA[+]	9.74	6.67	51.07	23.77	20.32	22.07	18.87	47.48	13.5/86.5	14.8/85.2
3B	**Metalast	11.00	5.34	53.04	22.59	14.22	23.99	21.74	48.08	15.4/84.6	16.8/83.2
3C	***Dipsol	12.79	6.76	58.15	27.59	14.46	28.01	14.59	37.64	16.6/83.5	18.1/81.9
3D	NA	12.42	6.67	50.79	23.77	13.70	22.07	23.09	47.32	17.3/82.7	18.9/81.0
3E	NA	14.38	7.15	51.21	22.99	14.91	26.30	19.50	43.56	19.1/81.0	20.7/74.3

* Refers only to Zn and Ni content. Other elements such as C, O, S were omitted.

** Commercial name: TCP-HF (Trivalent Cr chromate based)

*** Commercial name: IZ 258 (Hexavalent Cr chromate based)

[+] NA: Not Applied

The corrosion rates (Table 5.8) for laboratory air testing in tap water and NaCl solution show that coatings 3A and 3B exhibited comparable rates around 4-6 μA/cm^2. These values are consistent with the values obtained from Series 2 Zn-Ni coatings.

Comparing the behavior of the coatings 3B and 3C treated by conversion coatings, it is evident that only Metalast was effective in lowering the electrochemical potential and also the corrosion rate. Dipsol did not show a consistent behavior in affecting the corrosion potential. Both of these coatings had a lower Ni content compared to those in Series 2 that were treated with conversion coatings. Also, the morphological observations of the latter coatings suggested some specificity for these conversion coatings that were interacting either with the nodular or flake phase. Thus, the results suggest that the behavior of Dipsol may be composition dependent.

Table 5.8 Corrosion potential and corrosion rate values for Series 3 coatings in tap water and 3.5% NaCl under laboratory air and deaerated conditions.

	Laboratory Air Conditions				**Deaerated Conditions**			
Property	**E_{corr}**, mV		***i_{corr}***, μA/cm^2		**E_{corr}**, mV		***i_{corr}***, μA/cm^2	
Coating	Tap Water	3.5% NaCl	Tap Water	3.5% NaCl	Tap Water	3.5% NaCl	Tap Water	3.5% NaCl
3A	-596	-759	3.92	4.18	-649	-833	2.43	2.00
3B	-599	-879	4.55	5.88	-784	-862	1.08	3.56
3C	-563	-715	9.19	3.01	-564	-757	3.89	2.53
3D	-577	-731	4.64	5.50	-612	-747	1.52	1.90
3E	-568	-712	3.51	6.52	-651	-741	1.36	1.89
4340 Steel	-533	-728	9.20	320.88	-575	-760	1.60	0.92

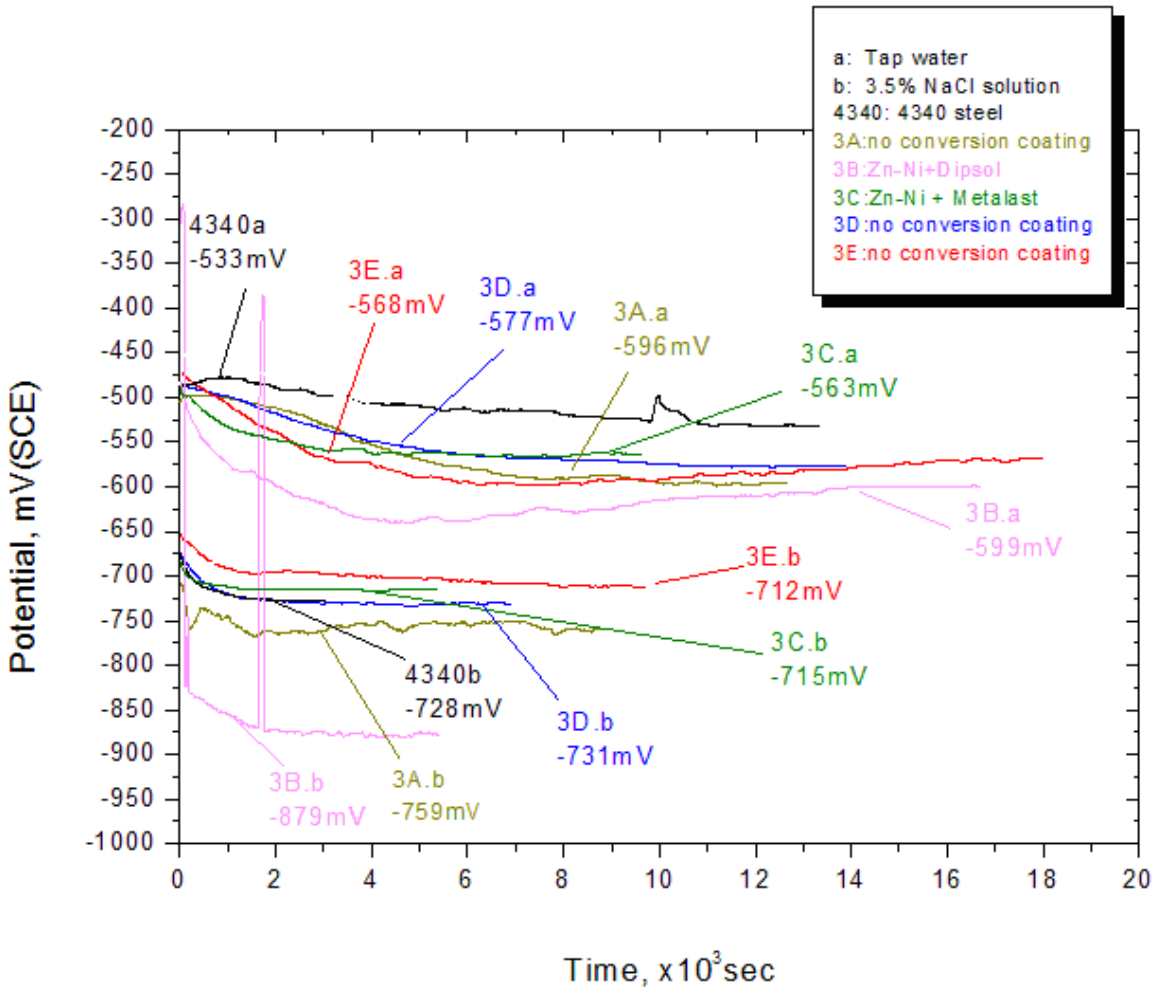

Figure 5.27 Variation of the corrosion potential as a function of immersion time for Series 3 coatings in both tap water and 3.5% NaCl solution under laboratory air conditions.

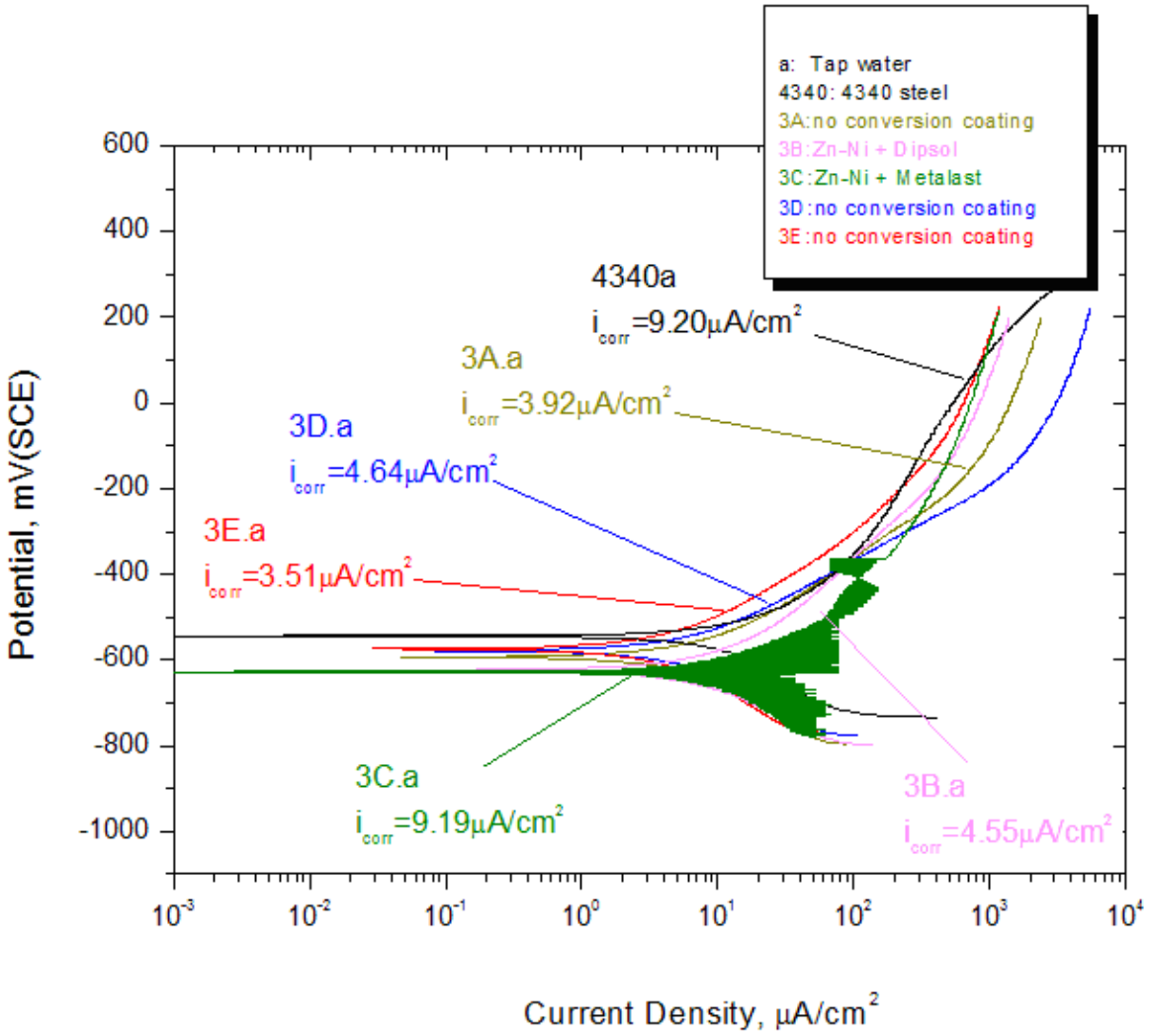

Figure 5.28 Anodic polarization behavior of Series 3 coatings in tap water under laboratory air conditions.

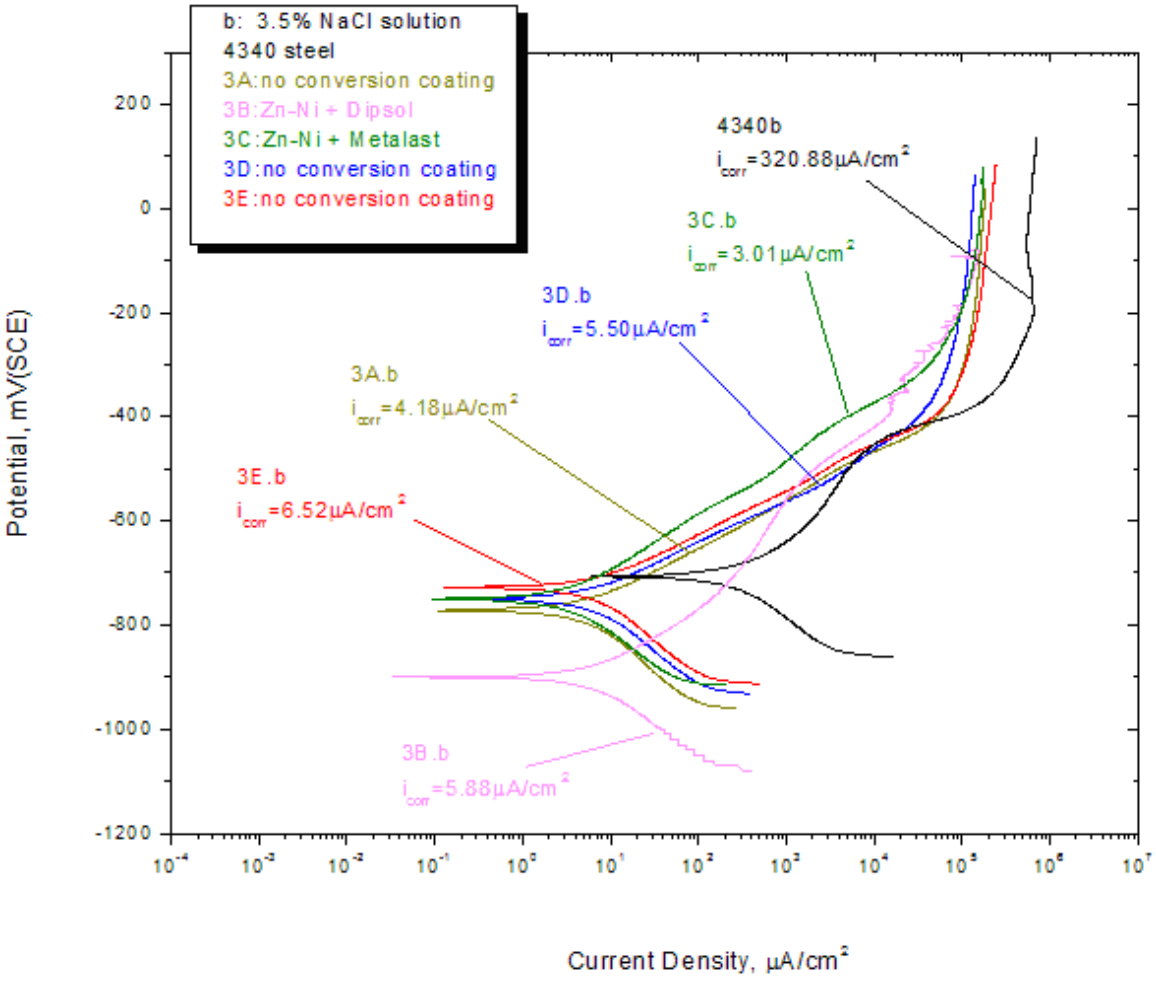

Figure 5.29 Anodic polarization behavior of Series 3 coatings in 3.5 % NaCl solution under laboratory air conditions.

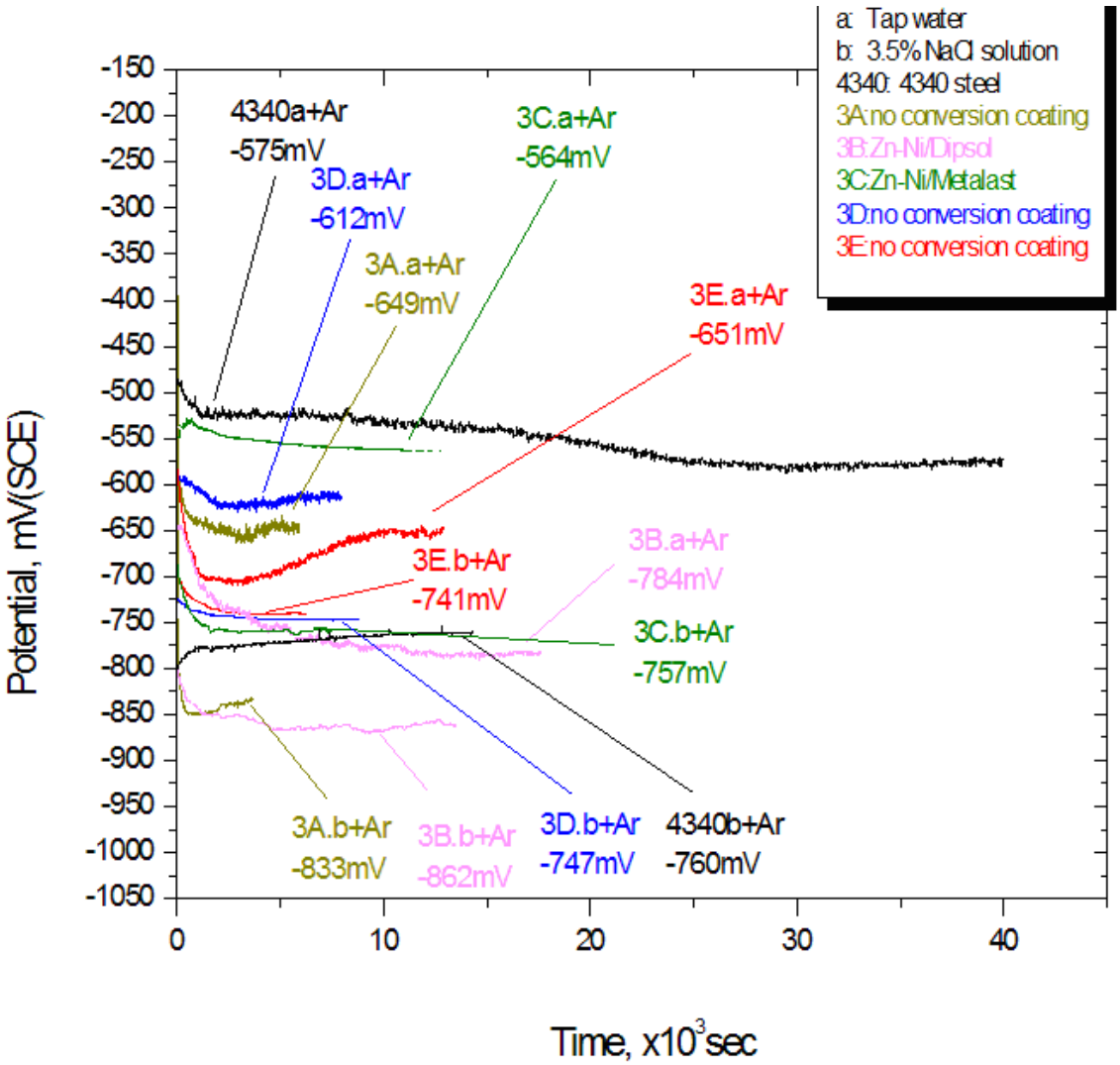

Figure 5.30 Variation of the corrosion potential as a function of immersion time for Series 3 coatings in both tap water and 3.5% NaCl solution under dearated conditions.

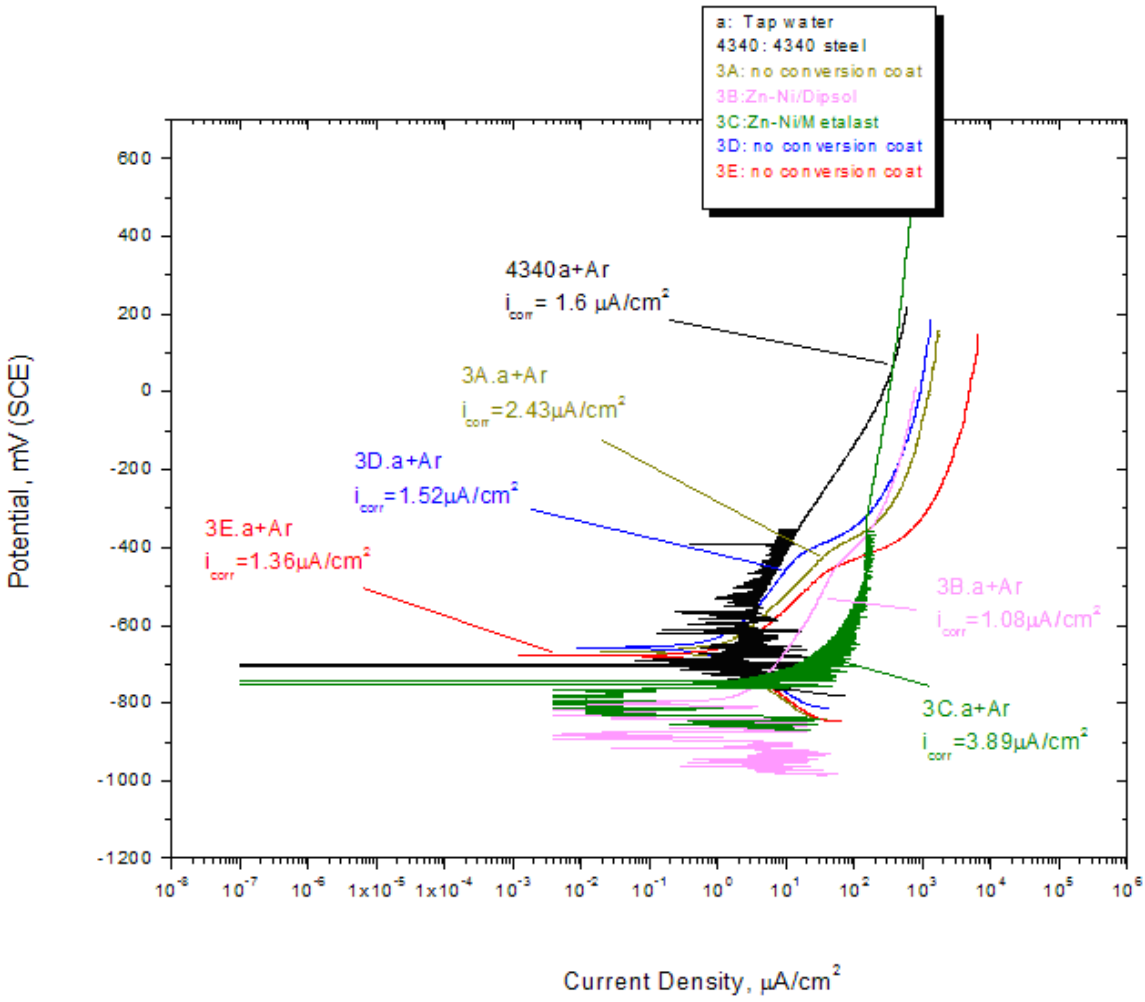

Figure 5.31 Anodic polarization behavior of Series 3 coatings in tap water under deaerated conditions.

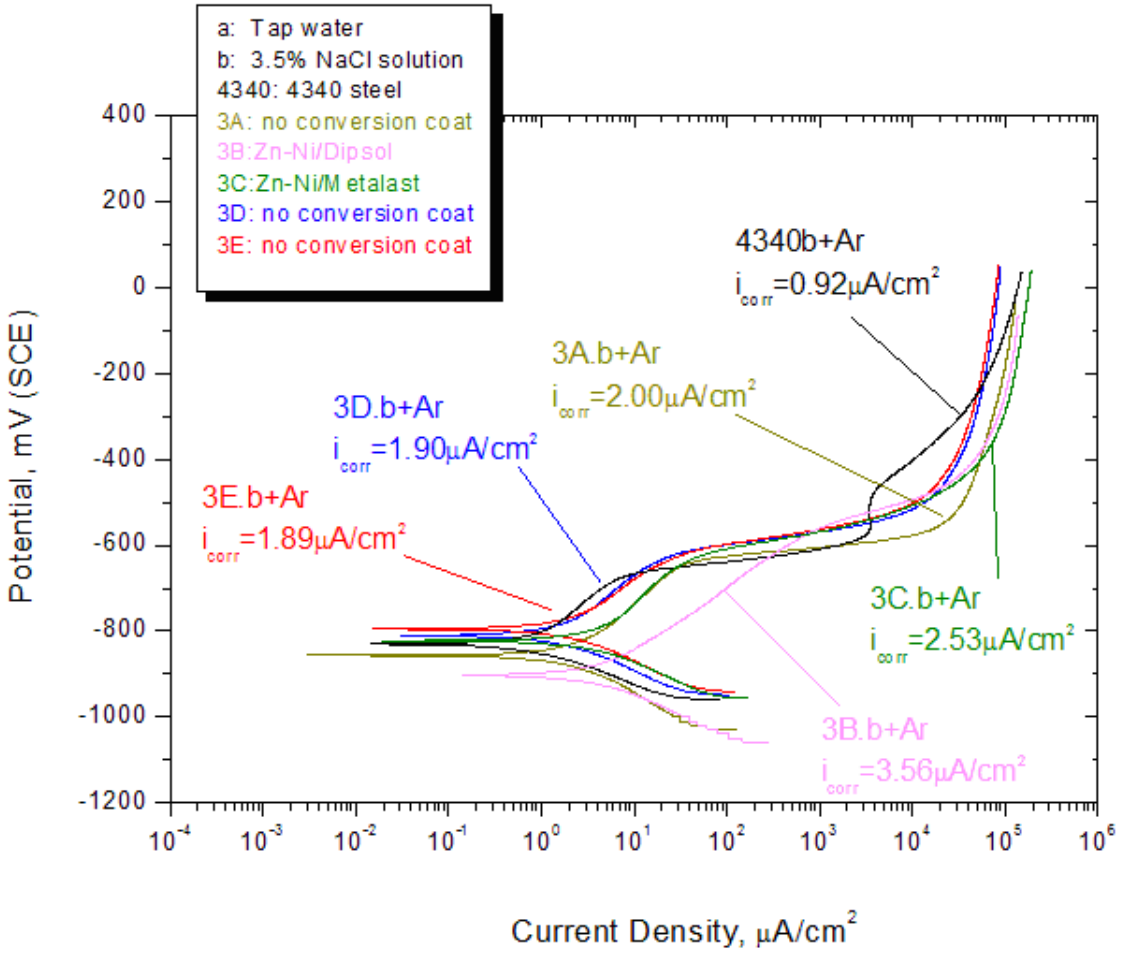

Figure 5.32 Anodic polarization behavior of Series 3 coatings in 3.5 % NaCl solution under deaerated conditions.

5.3.3 Salt fog corrosion testing

Twelve flat panels were Zn-Ni coated with the same conditions as those of coatings 3B (Metalast) and 3C (Dipsol) and tested under salt fog conditions at the NAVAIR Inorganic Coatings Laboratory (Patuxent, MD). The surface appearance of all panels was examined after 29 days of exposure. All panels treated with Dipsol exhibited significant corrosion. On the contrary, all Metalast treated panels were intact exhibiting excellent corrosion resistance. In view of that behavior, salt fog testing continued for 2700 hours. The Metalast treated panels continued to have an excellent performance even after this extended testing period. It is important to note that this behavior shown in an entirely different test is in complete agreement with the results from the laboratory experiments. Further more, the corrosion resistance shown by Metalast is significant since Dipsol is an agent containing hexavalent chromium while Metalast contains trivalent chromium and thus, it is not poisonous. Thus, the Metalast treatment of low Ni content Zn-Ni coatings provides excellent corrosion resistance while is environmentally friendly.

CHAPTER 6

CONCLUSIONS

- Nickel content in the Zn-Ni coatings can be effectively controlled in a wide range (from <15 to 30 wt. %) by manipulating the deposition variables of the EPP (i.e., Ni salt content in the electrolyte).
- Zn-Ni coatings deposited by EPP were found to be composed of two morphologically different phases, a nodular-type and a flake-type phase. XRD analysis showed that the nodular phase is a Zn-rich cubic phase whereas the flake-type is Ni-rich with a tetragonal structure. The nodular phase was dominant in coatings with low Ni contents whereas the flake phase dominated in high Ni content coatings. For lower Ni content, both phases are capable of dissolving Zn and Ni in similar quantities. Once a Ni content threshold is surpassed, the flake phase is capable of dissolving more Ni than the granular phase.
- EPP deposited Zn-Ni coatings are capable of offering electrochemical protection to underlying steel as long as the Ni content remains below ~20 wt%. Increasing the Ni content increases the electrochemical potential of the coating that becomes cathodic with respect to steel. Such coatings can't act as sacrificial anodes for corrosion protection.
- The conversion coatings were found to generally lower the corrosion potential of the Zn-Ni coatings. Further more, a particular conversion coating (Metalast) was found to lower both corrosion potential and corrosion rate. This behavior was found to be consistent in both laboratory experiments and aggressive salt fog testing. Thus, low Ni content Zn-Ni coatings treated with Metalast offer excellent corrosion protection while they are environmentally friendly.
- Low Ni content Zn-Ni coatings deposited by EPP showed great potential to serve as alternatives to electrodeposited Cd replacement.

REFERENCES

1. D. LANDLOT, *Corrosion and Surface Chemistry of Metals*, EPFL Press, Boca Raton, 2003.

2. P. GANESAN, S. KUMARAGURU, and B. POPOV, *Surf. Coat. Technol.,* 201 (2007) 7896.

3. S. YOU, G. PRATHEESH, and E. MELETIS, *Structure of Zinc-Nickel Coatings by using Electrolytic Plasma Processing*, Department of Materials Science and Engineering, Texas, 2007.

4. E. MELETIS, X. NIE, F. WANG, and J. JIANG, *Surf. Coat. Technol.*, 150 (2002) 246.

5. D. RICKERBY, and A. MATTHEWS, *Advanced Surface Coatings,* Chapman and Hall, New York. 1991.

6. http://corrosion.ksc.nasa.gov/corr_fundamentals.htm 06/0808

7. M. FONTANA, *Corrosion Engineering,* Third edition, Mcgraw-Hill, New York, 1986.

8. D. JONES, *Principles and Prevention of Corrosion,* Prentice Hall, Second edidition, New Jersey, 1996.

9. E. GREENER, P. HARDCOURT, and J. LAUTENSCHIEGER, *Materials Science and Engineering,* Williams and Wilkins Company, Chicago, 1972.

10. N. PEREZ, *Electrochemistry and Corrosion Science,* Kluwer, Puerto Rico, 2004.

11. E. BARDAL, *Corrosion and Protection,* Springer editors, United Kingdom, 2004.

12. D. ASKELAND, and P. PHULE, *The Science and Engineering of Materials*, Fourth edition, Thomson Books/Cole, California, 2003.

13. www.chemistry.nmsu.edu/studntres/chem435/Lab14/double_layer.gif 01/05/08

14. C. METZ, *Schaum Outline Series Theory and Problems of Physical Chemistry,* McGraw-Hill, San Francisco, 1976.

15. W. CALLISTER*, Fundamentals of Materials Science and Engineering,* Wiley and Songs, Second edition, 2005.

16. Z. PILB´ATH, and L. SZIR´AKI, *Electrochim. Acta*, 53 (2008) 3218.

17. G. WRANGLEN, *An Introduction to Corrosion and Protection of Metals,* Chapman and Hall, 1985.

18. A. STRAVOS, *Metals Handbook*, 9th edition, ASM international, OH, 1987.

19. D. BAYLISS, and D. DEACON, *Steelwork Corrosion Control,* Taylor and Francis group, New York, 2002.

20. A. TRACTON, *Coatings Materials and Surface Coatings,* Taylor and Francis Group, Boca Raton, 1986.

21. F. LAQUE, and N. GREENE, *Corrosion Basics: An Introduction*, National Association of Corrosion Engineering, Houston, 1978.

22. M. STERN, and C. MAKRIDES, *J. Electrochem. Soc.,* 107 (1960) 782.

23. D. TALBOT, and J. TALBOT, *Corrosion Science and Technology*, CRC Press, Boca Raton, 1998.

24. K. SESHAN, *Handbook of Film Deposition: Processes and Technologies,* Second edition, Noyes, California, 2002.

25. E, STANSBURY, and R. BUCHNAN, *Fundamentals of Electrochemical Corrosion,* ASM international, Ohio, 2000.

26. V. CARTER, *Metallic Coatings for Corrosion Control*, Newnes-Butterworths, 1977.

27. R. KREPSKI, *The Influence of Bath Alloy Additions in Hot-Dip Galvanizing*, St. Joe Minerals Corporation, 1980.

28. R. BANDY, *Corrosion Manual,* Florida, 1976.

29. http://en.wikipedia.org/wiki/Coatings 01/30/08

30. E.I. MELETIS, *Electrolytic Plasma Processing for Sequential Cleaning and Costing Deposition for Cadmium Plating Replacement,* Final Report, SERDP*,* 2005.

31. J. WACHTMAN, and R. HABER, *Ceramic Films and Coatings,* Noyes, 1993.

32. Y. LIN, and J. SELMAN, *J. Electrochem. Soc.,* 140 (1993) 1299.

33. T.FUKUMIZU, F. KOTANI, A. YOSHIDA, and A. KATAGIRI*, J. Electrochem. Soc.,* 153 (2006) C629.

34. www.asminternacional.org 09/07/08

35. A. EL HAJJAMI, M. GIGANDET, M. PTRIS-WERY, J. CATONNE, B. DUPRAT, L. THIERY, F. RAULIN, N. POMMIER, B. STARCK, and P. REMY, *Appl. Surf. Sci*., 254 (2007) 480.

36. A. ZHANG, *Surf. Tech.,* 26 (1997) 16.

37. J. CAI, and S. ZHOU, *Electroplating & Pollution Control,* 1993.

38. X. HU, and A. MAOZHONG , *Journal of Harbin Institute of Technology*, USA, 1985.

39. Y. LIN, and R. SELMAN*, J. Electrochem. Soc*., 140 (1993) 1299.

40. R. RAMANAUSKAS, P. QUINTANA, L. MALDONADO, and R. POMES, *Surf. Coat. Technol*., 92 (1997) 16.

41. V. RAMAN, B. PUSHPAVANAM, and A. SHENOI, *Met. Finish*., 81 (1983) 85.

42. G. LI, J. LIAN, L. NIU, and Z. JIANG*, Surf. Coat. Technol.,* 191 (2005) 59.

43. T. BYK, T. GAEVSKAYA, and L. TSYBULSKAYA, *Surf. Coating. Technol*., 54 (2008) 132.

44. E. BELTOWSKA-LEHMAN, P. OZGA, Z. SWIATEK, and C. LUPI, *Influence of Structural Factor on Corrosion Rate of Functional Zn-Ni Coatings,* Crystal engineering, 2002.

45. D. HALL, *Plat. Surf. Finish*., 70 (1983) 59.

46. T. VAGRAMYAN, V. HARLAMOV, and B. KUDRYAVTSEV, *Russ. Protec. Met.,* 32 (1996) 389.

47. G. BARCELO, J. GARCI, M. SARRET, and C. MULLER, *J. Appl. Electrochem*., 28 (1998) 1113.

48. J. HORKANS, *J. Electrochem. Soc.,* 128 (1981) 45.

49. I. CHASSANG, and R. WIART, *Electrochim. Acta*, 37 (1992) 545.

BIOGRAPHICAL INFORMATION

Giancarlo Rios was born on August 12 of 1980 in Caracas, Venezuela. He received his Bachelor of Science in Materials Science, from Simon Bolivar University, Venezuela in September 13, 2006. He began graduate work in the Materials Science and Engineering program at the University of Texas at Arlington, U.S.A. where he is currently a candidate for the degree of Master of Science and Engineering of Materials Science to be awarded at the Fall commencement, 2008.